Molecular and Cellular Neuroscience 39 (2008) 384–399

Contents lists available at ScienceDirect

Molecular and Cellular Neuroscience

journal homepage: www.elsevier.com/locate/ymcne

Correlation of T-channel coding gene expression, I_T, and the low threshold Ca^{2+} spike in the thalamus of a rat model of absence epilepsy

Tilman Broicher, Tatyana Kanyshkova, Patrick Meuth, Hans-Christian Pape, Thomas Budde *

Institut für Physiologie I, Westfälische Wilhelms-Universität Münster, Robert-Koch-Str. 27a, D-48149 Münster, Germany

ARTICLE INFO

Article history:
Received 22 April 2008
Revised 27 June 2008
Accepted 16 July 2008
Available online 29 July 2008

Keywords:
Patch clamp
T-type Ca2+ channel
Absence epilepsy
Thalamus
Burst firing
Real-time PCR

ABSTRACT

T-type Ca^{2+} current-dependent burst firing of thalamic neurons is thought to be involved in the hypersynchronous activity observed during absence seizures. Here we investigate the correlation between the expression of T-channel coding genes (α1G, -H, -I), T-type Ca^{2+} current, and the T-current-dependent low threshold Ca^{2+} spike in three functionally distinct thalamic nuclei (lateral geniculate nucleus; centrolateral nucleus; reticular nucleus) in a rat model of absence epilepsy, the WAG/Rij rats, and a non-epileptic control strain, the ACI rats. The lateral geniculate nucleus and centrolateral nucleus were found to primarily express α1G and α1I, while the reticular thalamic nucleus expressed α1H and α1I. Expression was higher in WAG/Rij when compared to ACI. The T-type Ca^{2+} current properties matched the predictions derived from the expression pattern analysis. Current density was larger in all nuclei of WAG/Rij rats when compared to ACI and correlated with LTS size and the minimum LTS generating slope, while T-type Ca^{2+} current voltage dependency correlated with the LTS onset potential.

Introduction

The thalamocortical system displays low frequency oscillatory activity during slow wave sleep as well as spike and wave discharges (SWD) observed during episodes of absence epilepsy (Avoli et al., 2001; Crunelli and Leresche, 2002; Steriade, 1997). The neural substrates of these slow oscillations are the thalamus and the cortex. Based on efferent projections, the thalamus can be divided into three groups of nuclei: (1) the specific nuclei, which project to well circumscribed cortical regions (e.g. lateral geniculate nucleus, LGN); (2) the non-specific nuclei, which project to broader, primarily frontal cortical regions and the striatum (e.g. centrolateral nucleus of the intralaminar nuclei, CL); (3) the reticular thalamic nucleus (NRT), which projects onto thalamocortical relay nuclei in an inhibitory manner, serving as a pacemaker.

Within the thalamus, the slow oscillations are accompanied by burst firing in thalamocortical relay (TC) as well as reticular neurons (Paz et al., 2007; Pinault et al., 1998; Seidenbecher and Pape, 2001; Seidenbecher et al., 1998; Slaght et al., 2002; Williams, 1953). Burst firing in thalamic neurons depends on the action of T-type Ca^{2+} channels. These channels generate a low threshold Ca^{2+} spike (LTS), which triggers a high frequency burst of action potentials (Huguenard, 1996). Until now, three genes (CACNA1G, -H, -I) coding for three T-type Ca^{2+} channel isoforms, termed α1G, α1H, and α1I, have been identified (Perez-Reyes, 2003). All isoforms seem to be subjected to alternative splicing, thus vastly increasing the number of physiologically distinct channel types (Perez-Reyes, 2006). Currents generated by the α1G and α1H isoforms appear rather similar in heterologous expression systems, while currents generated by the α1I isoform differ in voltage dependency and kinetics (Chemin et al., 2002).

Previous studies have shown that neurons of different thalamic nuclei (specific relay nuclei vs. reticular nucleus) display different T-type Ca^{2+} currents (I_T) and different LTS properties (Huguenard, 1996). In line with these findings, expression of T-channel isoforms has been found to vary between thalamic nuclei: relay nuclei primarily express the α1G isoform, while α1H and α1I expression has been observed in the NRT (Talley et al., 1999).

Several lines of evidence link thalamic I_T to slow oscillations of the thalamocortical system. Genetic rat models of absence epilepsy reveal an increased I_T and an increased expression of T-channel coding genes in the NRT (Talley et al., 2000; Tsakiridou et al., 1995). Knock-out mouse models have demonstrated the dependence of slow sleep oscillations as well as spike and wave discharges on the presence of the α1G isoform in the thalamus (Anderson et al., 2005; Kim et al., 2001; Song et al., 2004). Furthermore, anti-epileptic medications effective in human patients have been shown to suppress thalamic T-type Ca^{2+} currents (Broicher et al., 2007b; Coulter et al., 1989a,b; Leresche et al., 1998).

This study was designed to investigate the correlation between the expression of T-type Ca^{2+} channel coding genes, I_T, and the LTS in thalamic neurons. To include neuronal populations known to display differences in these parameters, neurons from LGN and NRT were

* Corresponding author. Fax: +49 251 83 55551.
E-mail address: tbudde@uni-muenster.de (T. Budde).

1044-7431/$ – see front matter © 2008 Elsevier Inc. All rights reserved.
doi:10.1016/j.mcn.2008.07.012

investigated. To extend the experiments to a neuronal population of largely unknown function and cellular properties, but a potential role in spreading epileptic activity throughout the thalamocortical system, CL neurons of the non-specific intralaminar nuclei have been included in the study. To scrutinize the effects of differences in the expression of T-type Ca^{2+} channel coding genes, I_T, and the LTS with respect to absence epilepsy all experiments have been performed in a genetic rat model of absence epilepsy, the WAG/Rij rats, and a non-epileptic control strain, the ACI rats (Coenen and Van Luijtelaar, 2003) by combining quantitative RT-PCR, whole-cell patch clamping in brain slices, and computer modeling.

Results

Expression pattern of CACNA1G, -H, -I transcripts in the LGN, CL, and NRT of WAG/Rij and ACI rats

First, the expression profile of the three T-type Ca^{2+} channel coding genes was examined in the LGN, CL, and NRT of WAG/Rij and ACI rats. Samples of tissue yielded through laser capturing were subjected to quantitative RT-PCR procedures (Fig. 1A, note that lower ΔCt values indicate higher mRNA expression). Distinct differences in gene expression were found between nuclei and strains. In the LGN and CL of both strains the CACNA1G isoform was strongly expressed, while only a weak signal could be detected in the NRT. In both LGN and CL, expression levels of the CACNA1G transcript were significantly higher in WAG/Rij than in ACI rats (Fig. 1B, Table 1).

The CACNA1H isoform was usually below detection limits in the CL and LGN, but was strongly expressed in the NRT of both strains and expression levels tended to be higher in WAG/Rij, although this trend failed to reach significance (Fig. 1C, Table 1).

The CACNA1I transcript was found to be expressed in all three nuclei of both strains. The expression levels were significantly different between strains and nuclei. The CL and NRT of WAG/Rij rats expressed significantly higher levels of CACNA1I mRNA than the same nuclei of ACI rats. Within each strain, CACNA1I expression was significantly higher in the NRT than in the CL and LGN, while expression in the CL was significantly higher than in the LGN (Fig. 1D, Table 1). A previous study by our group has demonstrated that the expression of CACNA1I can be attributed to the local circuit interneurons in the LGN. Thalamocortical projection neurons of the LGN (LGN TC), which were subjected to electrophysiological

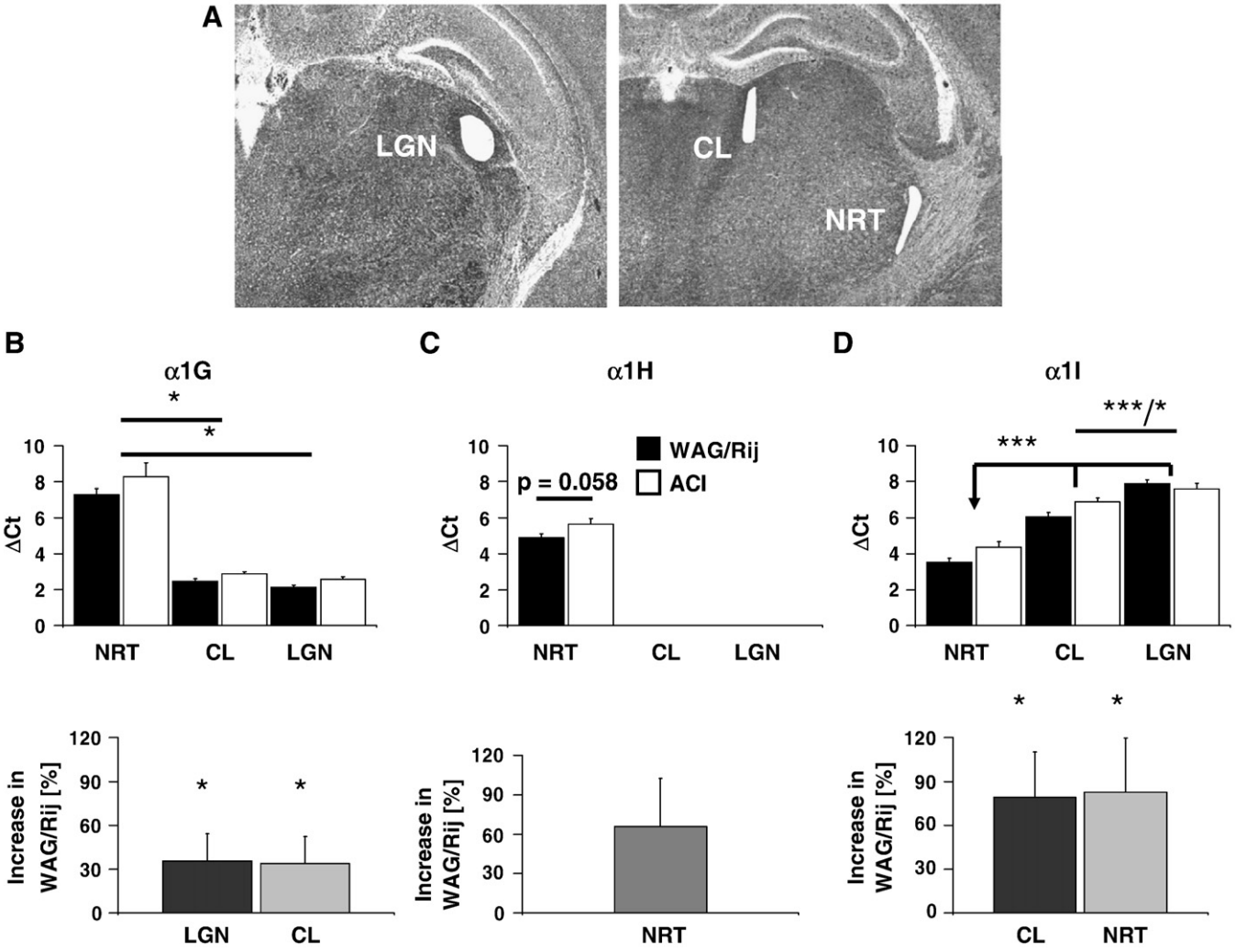

Fig. 1. Tissue level RT-PCR of CACNA1G, -H, and -I expression in the LGN, CL, and NRT of WAG/Rij and ACI rats. All 3 T-channel coding genes revealed an increased expression in WAG/Rij. Note that lower ΔCt values indicate higher mRNA expression. (A) Examples of brain slices after laser microdissection of LGN (left panel), CL (right panel) and NRT (right panel) tissue. (B) Mean cycle of threshold differences between CACNA1G and β2M mRNA in the LGN, CL, and NRT of WAG/Rij and ACI rats (upper panel). The increased CACNA1G expression in WAG/Rij as compared to ACI is depicted in the lower panel. (C) Mean cycle of threshold differences between CACNA1H and β_2-microglobuline (β2M) mRNA in the NRT of WAG/Rij and ACI rats (upper panel). CACNA1H expression was usually below the detection limit in the CL and LGN of both strains. In the lower panel the increased CACNA1H expression in WAG/Rij as compared to ACI is shown. (D) Mean differences of threshold circles from CACNA1I and β2M mRNA in the LGN, CL, and NRT of WAG/Rij and ACI rats (upper panel). The lower panel depicts the increased CACNA1I expression in WAG/Rij as compared to ACI. *$p<0.05$; **$p<0.01$; ***$p<0.001$.

Table 1
Summary of RT-PCR data and statistical analysis

	CACNA1G [ΔCt]	CACNA1H [ΔCt]	CACNA1I [ΔCt]
WAG/Rij LGN	2.1±0.1; $n=12$	//	7.9±0.2; $n=12$
CL	2.5±0.1; $n=12$	//	6.1±0.2; $n=12$
NRT	7.3±0.3; $n=12$	4.9±0.2; $n=12$	3.5±0.2; $n=12$
ACI LGN	2.6±0.1; $n=13$	//	7.6±0.3; $n=13$
CL	2.9±0.1; $n=12$	//	6.9±0.2; $n=12$
NRT	8.3±0.8; $n=12$	5.6±0.3; $n=12$	4.4±0.3; $n=12$
Statistical significances CACNA1G			
	LGN vs. CL	LGN vs. NRT	CL vs. NRT
WAG/Rij	N.S.	*	*
ACI	N.S.	*	*
	LGN vs. LGN	CL vs. CL	NRT vs. NRT
WAG/Rij vs. ACI	*	*	N.S.
*$p<0.05$; **$p<0.01$; ***$p<0.001$.			
Statistical significances CACNA1H			
	LGN vs. CL	LGN vs. NRT	CL vs. NRT
WAG/Rij	//	//	//
ACI	//	//	//
	LGN vs. LGN	CL vs. CL	NRT vs. NRT
WAG/Rij vs. ACI	//	//	N.S. ($p=0.058$)
*$p<0.05$; **$p<0.01$; ***$p<0.001$.			
Statistical significances CACNA1I			
	LGN vs. CL	LGN vs. NRT	CL vs. NRT
WAG/Rij	***	***	***
ACI	*	***	***
	LGN vs. LGN	CL vs. CL	NRT vs. NRT
WAG/Rij vs. ACI	N.S.	*	*
*$p<0.05$; **$p<0.01$; ***$p<0.001$.			

N.S.: not significant.

investigation in this study, solely express the CACNA1G gene (Broicher et al., 2007a).

Next, the possibility of alternative splicing of the CACNA1G transcript (exons 25/26) was investigated in the CL of both strains. Alternatively spliced CACNA1G transcripts have been shown to give rise to physiologically distinct channels (Chemin et al., 2001; Emerick et al., 2006) and have been implicated in the generation of the diverging T-type Ca^{2+} currents of LGN projection and local circuit interneurons (Broicher et al., 2007a). Non-quantitative RT-PCR experiments on CL tissue samples gathered through laser dissection microscopy revealed the presence of two alternatively spliced isoforms in the CL, data not shown. The smaller isoform will be referred to as Iso1 (analogous to human α1G-a, AF027984), the larger isoform will be referred to as Iso2 (analogous to human α1G-bc, AF125161). In the majority of CL tissue samples from both strains bands corresponding to both isoforms could be detected (WAG/Rij CL: Iso1 only: 1 of 7 samples, Iso2 only: 0 of 7 samples; Iso1 and Iso2: 6 of 7 samples; ACI CL: Iso1 only: 2 of 8 samples, Iso2 only: 1 of 8 samples, Iso1 and Iso2: 5 of 8 samples; data not shown).

Assuming that the differences on the mRNA level translate into differences in channel protein, these results allow some predictions concerning the properties of the T-type Ca^{2+} currents. The increased expression of T-channel coding mRNA could lead to an increase in I_T density in WAG/Rij. According to data from heterologous expression systems (Chemin et al., 2001, 2002; Emerick et al., 2006), NRT neurons of both strains should display a T-type Ca^{2+} current voltage dependency of comparatively positive values and slow kinetics, while the I_T of LGN TC neurons should display a rather negative I_T voltage dependency and fast kinetics. The I_T of CL neurons should be of intermediate voltage dependency and kinetics, when compared to the I_T recorded in LGN TC and NRT neurons.

Electrophysiological properties of T-type Ca^{2+} currents in LGN, CL, and NRT neurons of WAG/Rij and ACI rats

To correlate I_T of LGN TC, CL, and NRT neurons of WAG/Rij and ACI rats with the expression of the T-channel coding genes and the LTS, the T-type Ca^{2+} current properties were investigated. Whole-cell voltage clamp techniques were employed on neurons in brain slice preparations. Between the stimulation protocols neurons were held at −60 mV.

Voltage dependency of activation

The steady-state voltage dependency of activation was investigated by stepping neurons to increasingly positive test potentials (200 ms, CL and LGN; 500 ms, NRT) from a conditioning potential of −110 mV (700 ms, all nuclei; Fig. 2A). Construction of steady-state activation curves revealed half maximal activation voltages (V_h), which were significantly different between nuclei and strains (Fig. 2B). In both strains, the T-type Ca^{2+} current of LGN TC neurons activated at the most negative potentials, followed by neurons of the CL, where I_T activated at intermediate potentials, and neurons of the NRT, whose T-type Ca^{2+} currents activated at the most positive voltages (Fig. 2B, Table 2). The steady-state activation curves of the T-type Ca^{2+} currents recorded in LGN and CL relay neurons of WAG/Rij rats revealed significantly more negative V_h values when compared to the corresponding V_h values obtained from recordings in neurons of ACI rats. In the NRT the opposite situation was observed. Here, the V_h values of steady-state activation revealed a small but significant shift towards more positive potentials in WAG/Rij when compared to ACI (Table 2).

Voltage dependency of inactivation

In the following, the steady-state inactivation was investigated by holding neurons at increasingly positive potentials, starting from −110 mV (700 ms, all nuclei), and stepping to a constant analyzing potential of −55 mV (200 ms, CL and LGN; 500 ms, NRT; Fig. 2C). As found for the steady-state activation, the half maximal voltages of steady-state inactivation revealed significant differences between strains and nuclei (Fig. 2D). In WAG/Rij, the T-type Ca^{2+} currents recorded in LGN TC neurons inactivated at the most negative potentials, followed by T-type Ca^{2+} currents recorded in CL neurons, and by T-type Ca^{2+} currents of NRT neurons, which inactivated at the most positive potentials. In ACI, the inactivation voltage dependencies of LGN TC and NRT neurons were similar, while CL neurons displayed more positive voltage dependencies of inactivation (Table 2). A comparison between strains proved the differences between the steady-state inactivation V_h of WAG/Rij and ACI CL and NRT to be significant. Within the WAG/Rij strain the differences between the inactivation V_h of all three nuclei were significant, while in ACI rats only the difference between CL and NRT was found to be significant ACI (Table 2).

Current density

As differences in T-type Ca^{2+} current density have been observed in other models of absence epilepsy, the maximal amplitudes and T-type Ca^{2+} current densities evoked by the activation type protocol have been compared between nuclei and strains. Within both strains, CL neurons displayed the highest T-type Ca^{2+} current amplitude, followed by the LGN, and the NRT. All differences in T-type Ca^{2+} current amplitudes between nuclei were significant within strains. Between strains, differences were significant for I_T amplitudes of LGN TC and CL neurons (Fig. 3A; Table 2). To obtain a measure of channel density per unit area of cell membrane, the T-type Ca^{2+} current amplitudes were divided by the capacitance of the neurons. Within and between both strains, capacitances of relay neurons of the LGN and CL were indistinguishable, while neurons of the NRT displayed significantly smaller capacitances than relay neurons of the LGN and

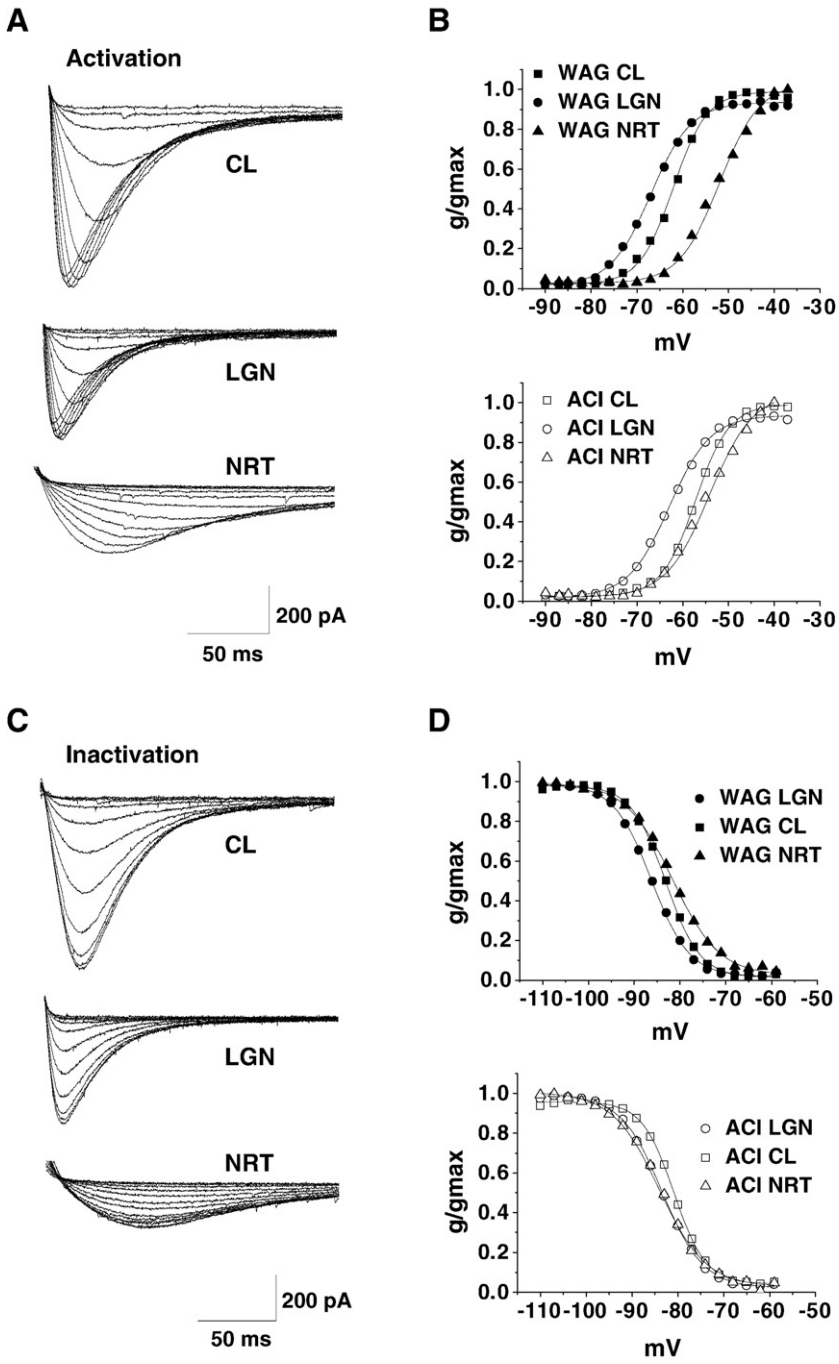

Fig. 2. Voltage dependency of activation and inactivation of T-type Ca^{2+} currents in LGN TC, CL, and NRT neurons of WAG/Rij and ACI rats. (A) Representative families of I_T of a LGN TC, a CL, and a NRT neuron. Displayed recordings derive from neurons taken from ACI rats. Neurons were clamped to increasingly positive test potentials from a holding potential of −110 mV. The initial test potential was −90 mV, which was increased in steps of 3 mV. (B) Activation curves from LGN TC, CL, and NRT neurons of WAG/Rij (upper panel) and ACI rats (lower panel; symbols as indicated) were obtained by fitting a Boltzmann equation to plots of mean values of normalized peak conductance vs. the test potential. Standard error bars have been omitted for clarity; see Table 2 for statistical data. (C) Representative families of I_T in LGN TC, CL, and NRT neurons. Recordings derived from neurons of ACI rats are shown. Neurons were stepped to a constant analyzing potential of −55 mV from increasingly positive conditioning potentials. Initial conditioning potential was −110 mV, which was altered in increments of 3 mV. (D) Inactivation curves from LGN, CL, and NRT neurons of WAG/Rij (upper panel) and ACI rats (lower panel; symbols as indicated) were obtained by fitting a Boltzmann equation to plots of mean values of normalized peak conductance vs. the test potential. Standard error bars have been omitted for clarity; see Table 2 for statistical data.

CL (Table 2). Within both strains NRT neurons displayed the largest T-type Ca^{2+} current densities, followed by neurons of the CL and the LGN (Fig. 3B, Table 2). Within both strains, the T-type Ca^{2+} current densities of LGN TC neurons were significantly smaller than the T-type Ca^{2+} current densities recorded in CL and NRT neurons, while the differences between CL and NRT neurons were not significant. All T-type Ca^{2+} current densities were significantly increased in WAG/Rij compared to ACI (Fig. 3B, Table 2).

Activation and inactivation kinetics

Next, time-dependent activation and inactivation properties of the T-type Ca^{2+} currents recorded in LGN TC, CL, and NRT neurons were analyzed. The inactivation of T-type Ca^{2+} currents was complete in all nuclei of both strains. In WAG/Rij and ACI rats, the T-type Ca^{2+} current recorded in LGN TC neurons was fastest to activate and inactivate, followed by I_T recorded in the CL, which displayed intermediate kinetics, and the I_T of NRT neurons, which was slowest to activate and inactivate.

Table 2
Summary of electrophysiological data and statistical analysis

	WAG/Rij LGN TC	WAG/Rij CL	WAG/Rij NRT	ACI LGN TC	ACI CL	ACI NRT
I_T V_h act [mV]	−66±1.5; n=19	−62.3±1; n=24	−52±0.5; n=31	−61.7±1.4; n=24	−57.4±1; n=26	−54.4±0.5; n=40
I_T V_h inact [mV]	−86.1±1; n=18	−83.4±0.8; n=25	−81.6±0.3; n=30	−83.1±1.1; n=21	−80.8±0.7; n=24	−83.5±0.3; n=39
TTP at −61 mV [ms]	22.8±2; n=19	35.7±2; n=2	97±6; n=31	22.1±1; n=24	37.8±3; n=27	99.6±5; n=40
TTP at −37 mV [ms]	13±1; n=19	18±2; n=24	35.8±1; n=31	15±3; n=24	16.1±1; n=27	34.7±1; n=40
Inact τ at −61 mV [ms]	28.9±2; n=19	38.6±2; n=24	137.7±16; n=31	29.9±2; n=24	44.6±4; n=27	116.7±7; n=40
Inact τ at −37 mV [ms]	23.5±1; n=19	34.9±2; n=24	55±2; n=31	26.8±2; n=24	30.4±2; n=27	54.2±2; n=40
I_T peak amp [pA]	−647±37; n=29	−941±60; n=25	−421±28; n=28	−509±26; n=34	−703±53; n=25	−372±24; n=40
Capacitance [pF]	119±4; n=29	133±7; n=25	59±4; n=31	110±4; n=34	118±7; n=25	60±3; n=40
CD [pA/pF]	5.4±0.2; n=34	7.2±0.3; n=25	7.4±0.4; n=31	4.7±0.2; n=34	6.1±0.3; n=25	6.4±0.3; n=40
V_{Rest} [mV]	−72.6±1; n=29	−69.5±1; n=43	−75.6±1; n=21	−74.4±1; n=29	−70.7±1; n=35	−74.3±1; n=40
# LTS APs	2.4±0.2; n=25	2.3±0.2; n=39	9.9±1.7; n=21	2.4±0.2; n=25	1.8±0.2; n=26	10.4±1.2; n=39
LTS onset [mV]	−62.3±1; n=14	−63.8±1; n=19	−51.3±2; n=9	−65.8±1; n=13	−62.8±1; n=16	−53.6±2; n=12
LTS generating slope [mV/s]	8.3±0.5; n=14	4.8±0.6; n=18	5.3±0.5; n=9	11.5±0.8; n=13	5±0.6; n=16	4.6±0.4; n=12
Δ depolarization slopes	5.8±0.5; n=14	2.5±0.5; n=18	0.5±0.3; n=9	9.7±0.9; n=13	2.6±0.6; n=16	0.3±0.2; n=12
LTS generating slope TTX [mV/s]	17.2±4; n=3	6.4±1; n=3	13.6±2; n=3	20.9±2; n=3	10.7±3; n=3	20.1±4; n=3
Δ depolarization slopes TTX	14.1±4; n=3	2.9±1; n=3	8.3±1; n=3	17.4±2; n=3	7.1±3; n=3	13.9±4; n=3
LTS generating slope TTX/4-AP [mV/s]	3.9±0.4; n=11	4.0±0.5; n=9	5.2±0.2; n=12	5.6±0.6; n=9	4.9±0.9; n=11	4.9±0.5; n=9
Δ depolarization slopes TTX/4-AP	1.2±0.3; n=11	1.8±0.5; n=9	0.6±0.2; n=12	3.8±0.6; n=9	2.4±0.8; n=11	0.8±0.4; n=9

Statistical significances within strains

	WAG/Rij LGN vs. CL	WAG/Rij LGN vs. NRT	WAG/Rij NRT vs. CL	ACI LGN vs. CL	ACI LGN vs. NRT	ACI NRT vs. CL
I_T V_h act	*	***	***	*	***	**
I_T V_h inact	*	***	*	N.S.	N.S.	***
TTP	* to ***	***	***	* to ***	***	***
Inact τ	** to ***	***	***	** to ***	***	***
I_T peak amp	***	***	***	***	***	***
Capacitance	N.S.	***	***	N.S.	***	***
CD	***	***	N.S.	***	***	N.S.
V_{Rest}	*	N.S.	***	*	N.S.	*
# LTS APs	N.S.	***	***	N.S.	***	***
LTS onset	N.S.	***	***	*	***	***
LTS generating slope	***	**	N.S.	***	***	N.S.
Δ depolarization slopes	***	***	**	***	***	**

*p<0.05; **p<0.01; ***p<0.001.

Statistical significances between strains

	LGN	CL	NRT
I_T V_h act	*	**	**
I_T V_h inact	N.S.	*	***
TTP	N.S.	N.S.	N.S:
Inact τ	N.S.	N.S.	N.S.
I_T peak amp	**	**	N.S.
Capacitance	N.S.	N.S.	N.S.
CD	*	*	*
V_{Rest}	N.S.	N.S.	N.S.
# LTS APs	N.S.	N.S.	N.S.
LTS onset	*	N.S.	N.S.
LTS generating slope	**	N.S.	N.S.
Δ depolarization slopes	***	N.S.	N.S.

*p<0.05; **p<0.01; ***p<0.001.

Differences in current kinetics were minor between strains, but were found to be significant between nuclei. The time to maximum current amplitude was used as a measure of activation kinetics (Figs. 3C, D), while the time constants of inactivation were obtained by fitting the current traces with a mono-exponential function (Figs. 3E, F; Table 2).

In summary the predictions of the T-type Ca^{2+} current properties derived from the expression analysis have been validated for the differences in I_T voltage dependency of activation and the I_T kinetics between nuclei. While the internucleus variations were expected, the differences in voltage dependency between WAG/Rij and ACI were unexpected and cannot be explained by the T-channel isoform expression pattern or differential splicing of exons 25/26 investigated in this study. Furthermore, the increased expression of T-channel coding mRNA in WAG/Rij translated into increased I_T densities.

Predicting the influence of different I_T characteristics on the LTS

After having established the expression pattern of the pore forming T-type Ca^{2+} channel α1 subunits and the electrophysiological properties of T-type Ca^{2+} currents in LGN TC, CL, and NRT neurons of WAG/Rij and ACI rats, we focused our attention on the functional correlate of I_T, the LTS. There are a number of LTS parameters which could be directly determined by certain T-type Ca^{2+} current properties. Intuition predicts the LTS onset potential to correlate with the voltage dependency of I_T activation, while the number of LTS associated action potentials and the stimulation intensity required to generate a LTS should depend on the T-type Ca^{2+} current density.

To test the validity of these assumptions, a single compartment model based on the mathematical descriptions of I_T, $I_{Na\ HH}$, $I_{K\ HH}$, I_{NaP}, I_L, I_A, I_{KCa}, as well as a sodium and a potassium leak current was used (Broicher et al., 2007a). Two types of protocols were used to stimulate the model neuron in the current-clamp regime. To assess the influence of different I_T parameters on the number of LTS associated action potentials, a step depolarization protocol was used. The model cell was hyperpolarized to −100 mV for 800 ms, before being stepped to −70 mV, whereupon a LTS was generated. The influence of changes of I_T on the LTS onset potential and the stimulation intensity required to elicit a LTS was investigated using a current ramp protocol. Here, the

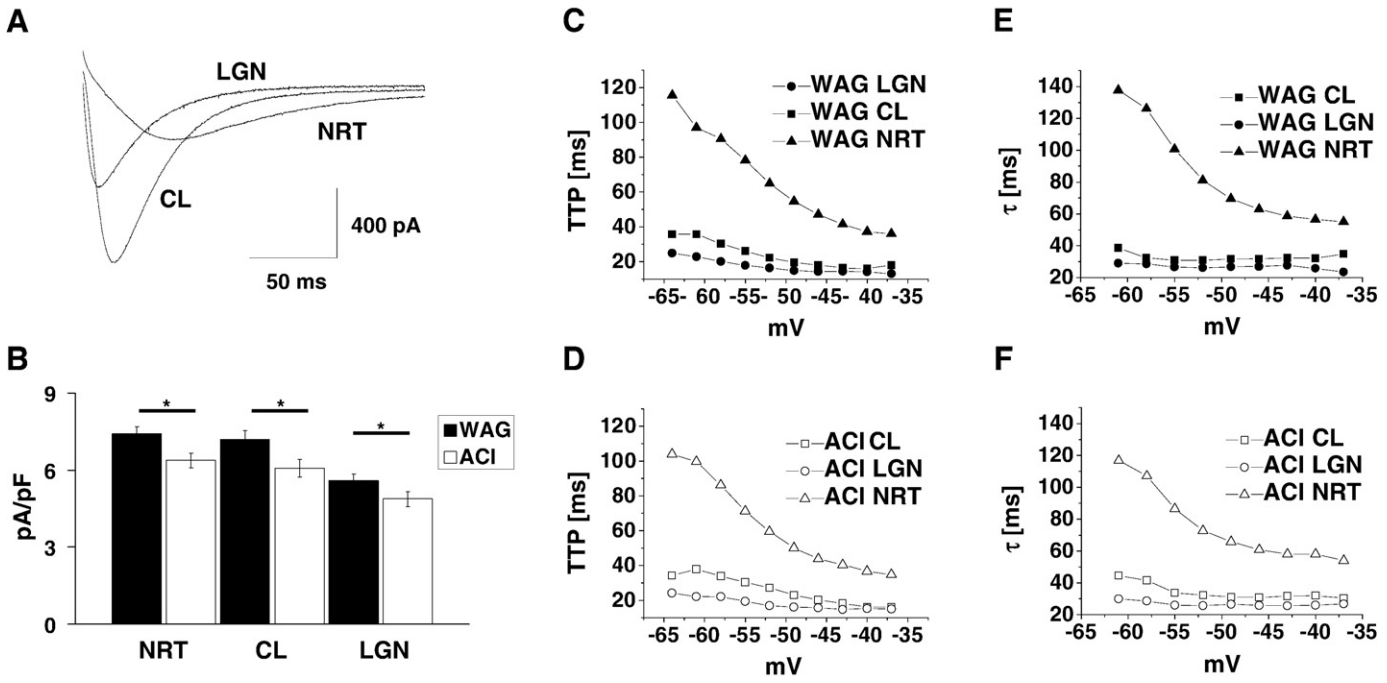

Fig. 3. T-type Ca^{2+} current density and current kinetics of LGN TC, CL, and NRT neurons of WAG/Rij and ACI rats. (A) Representative peak T-type Ca^{2+} currents of a LGN TC, a CL, and a NRT neuron. Displayed recordings derive from neurons taken from ACI rats. (B) I_T density of WAG/Rij and ACI LGN, CL, and NRT neurons. See text for statistical data. *$p<0.05$. (C) Mean values of the time to peak amplitude of T-type Ca^{2+} currents of WAG/Rij LGN TC, CL, and NRT neurons in relation to the activation protocol test potential (symbols as indicated). Standard error bars have been omitted for clarity. (D) Mean values of the time to peak amplitude of T-type Ca^{2+} currents of ACI LGN TC, CL, and NRT neurons in relation to the activation protocol test potential (symbols as indicated). (E) Mean values of the time constant of inactivation of WAG/Rij LGN TC, CL, and NRT neurons obtained by fitting of current traces with a mono-exponential function (symbols as indicated). (F) Mean values of the time constant of inactivation of ACI LGN TC, CL, and NRT neurons obtained by fitting of current traces with a mono-exponential function (symbols as indicated). Standard error bars have been omitted for clarity.

model neuron was held at −100 mV before being depolarized by current ramps of varying slopes. I_T parameters including the T-type Ca^{2+} current voltage dependency and current density were shifted by ±5 mV and ±30%, respectively.

Under control conditions (initial I_T configuration), the model neuron generated 4 LTS associated action potentials in response to current step stimulation (Fig. 4B). Increasing the T-type Ca^{2+} current density by 30% led to an increase in the number of action potentials to 5 (Fig. 4C, upper panel), while decreasing the T-type Ca^{2+} current density by 30% reduced the number of LTS associated action potentials to 3 (Fig. 4C, lower panel). The number of LTS associated action potentials was unaffected by hyperpolarizing the I_T voltage dependency by 5 mV, while a 5 mV depolarizing shift reduced the number of action potentials to 3 (Fig. 4A).

The LTS onset potential during current ramp stimulations was estimated by a threshold based algorithm using the first derivative of the voltage trace (see Experimental methods). We began the simulations using supra threshold stimuli and progressively decreased the stimulus intensity. This initially leads to the disappearance of the LTS associated action potentials followed by a gradual decline in LTS amplitude with weaker stimuli (data not shown). The first LTS without any associated action potentials was used for quantification. Under control conditions the model cell's LTS onset potential was −75.4 mV. Shifting the I_T voltage dependency by 5 mV in the negative direction resulted in a hyperpolarization of the LTS onset potential to −79.9 mV, while shifting the I_T voltage dependency by 5 mV in the positive direction depolarized the LTS onset potential to −68.1 mV (Fig. 4D). The effects of changes in I_T density on the LTS onset potential were comparatively minor (data not shown).

To investigate the effects of changes in I_T parameters on the stimulus intensity required for LTS generation, the depolarization slopes were investigated. The depolarization slopes were obtained by linearly fitting the simulated voltage trace between the start of the stimulation and the LTS onset point (as defined above). Again, the stimulation intensity was continuously decreased. The first LTS without any associated action potentials was used for quantification. Under control conditions, a depolarization slope of 42.6 mV/s generated the first LTS without associated action potentials. Shifting the I_T voltage dependency by 5 mV in the negative direction shifted the depolarization slope to 38.9 mV/s. Depolarizing the I_T voltage dependency by 5 mV increased the depolarization slope to 52.5 mV/s (data not shown). The effects of changes in I_T density on depolarization slopes were more pronounced than the effects of changes in I_T voltage dependency. Increasing the T-type Ca^{2+} current density by 30% reduced the depolarization slope to 28.1 mV/s. Decreasing I_T density by 30% increased the depolarization slope to 68.5 mV/s (Fig. 4E).

In summary, the LTS onset potential of the model neuron was dependent on the I_T voltage dependency, while the number of LTS associated action potentials and the stimulation intensity were dependent on the T-type Ca^{2+} current density. If the differences in T-type Ca^{2+} current properties directly translate into differences of the LTS onset potential in neurons of WAG/Rij and ACI rats recorded in the LGN, CL, and NRT, the model predicts that: (1) LTS onset potentials of LGN TC neurons should be negative to the LTS onset potentials of CL neurons in both strains. (2) LTS onset potentials of NRT neurons should be depolarized to the LTS onset potentials of LGN TC and CL neurons in both strains. (3) LGN and CL neurons of WAG/Rij should display LTS onset potentials negative to the LTS onset potentials of ACI LGN and CL neurons. (4) The LTS onset potential of NRT neurons of WAG/Rij and ACI rats should be approximately similar. Furthermore, the model predicts that neurons of the NRT should generate the most LTS associated action potentials, followed by neurons of the CL. LGN neurons should generate the least amount of LTS associated action potentials, due to the comparatively small I_T density. Analogous, neurons of WAG/Rij rats are predicted to generate more LTS associated action potentials than ACI neurons. A similar pattern should be

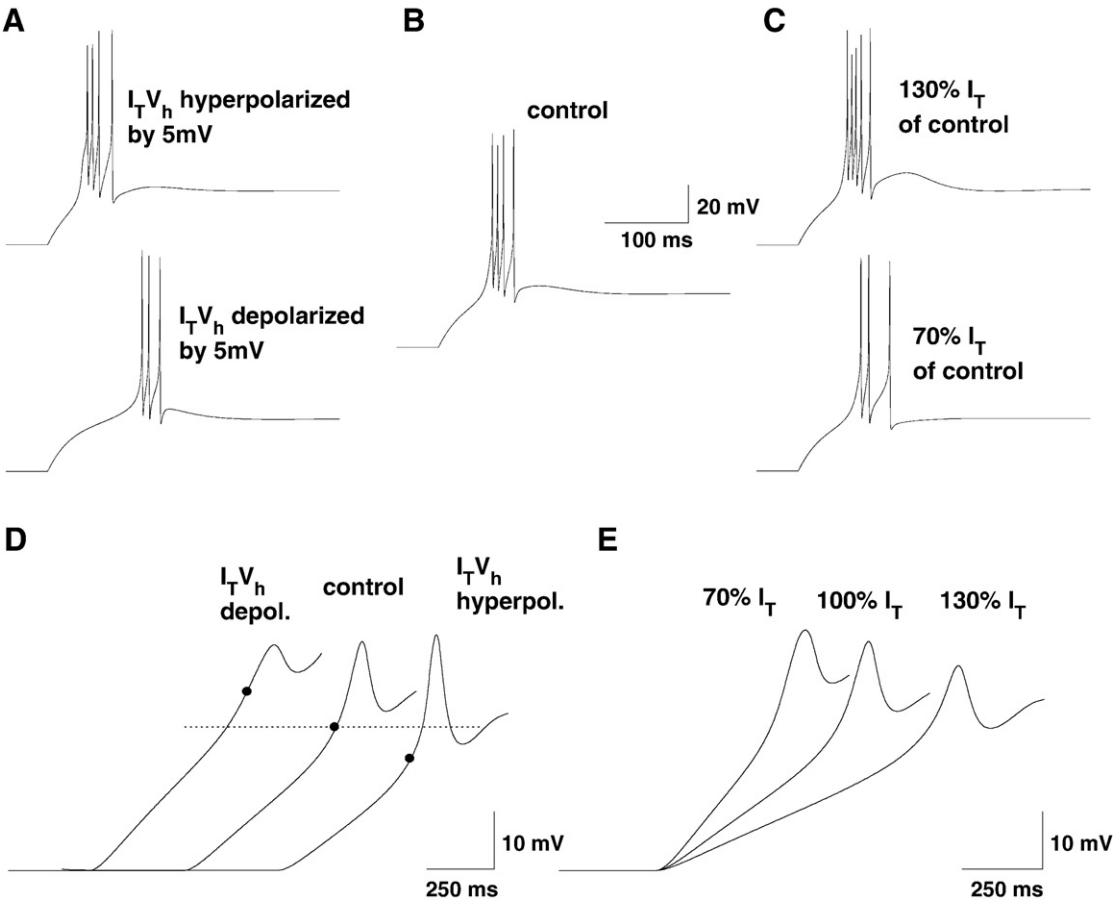

Fig. 4. The influence of the V_h of I_T activation as well as the T-type Ca^{2+} current density on the number of LTS associated action potentials of a model neuron is shown in A, B, and C. A current step protocol was used to elicit the LTS. The modeled LTS under control conditions is shown in (B). The influences of changes in V_h are depicted in (A). The upper panel displays the effect of a negative 5 mV shift of the I_T V_h on the LTS. The influence of a shift of 5 mV in the positive direction is shown in the lower panel. In (C) the effects of alterations of I_T density on the LTS are depicted. The upper panel shows a LTS generated by a modeled neuron with 130% of the control T-current density. In the lower panel a LTS generated in the presence of 70% of the control T-current density is displayed. In D and E the effects of alterations in I_T voltage dependency and current density on the LTS onset potential and the minimal LTS generating slope are displayed. Current ramp stimulations were used to elicit the LTS. The LTS onset potential was defined using the derivatives of the voltage traces (dV/dt) by a threshold based algorithm (see text). The simulations were started using above threshold depolarization slopes. Subsequently, the depolarization slopes were decreased by a fixed amount, until all LTS associated action potentials were lost. The first trace without any LTS associated action potentials was used for quantification (see text). (D) Effect of changes of the I_T voltage dependency on the LTS onset potential. LTS onset potentials are marked by black circles. A model with the initial I_T configuration is shown in the middle (control). On the left side the effect of a 5 mV depolarization of the I_T voltage dependency is shown, while the right side displays the effect of a 5 mV hyperpolarization. (E) Effect of changes in I_T density on the minimal LTS generating slope. A simulation using the initial I_T configuration is shown in the middle (100% I_T). On the left side, the effect of a reduction of the I_T density by 30% is shown. On the right the influence of an increase of the I_T density by 30% on the minimal LTS generating slope is depicted.

observed for the minimal stimulation intensity leading to LTS generation. NRT neurons should require the smallest depolarization slopes leading to LTS generation, while CL and LGN neurons should require stronger stimulation intensities.

Electrophysiological properties of LGN, CL, and NRT neurons of WAG/Rij and ACI rats

To test the predictions made by the mathematical model we went on to do whole-cell current-clamp recordings on neurons in brain slice preparations. The resting membrane potentials of neurons recorded in the same nucleus of WAG/Rij and ACI rats were similar. However, significant differences were found for the resting membrane potentials of neurons recorded in the different nuclei within both strains. Neurons of the CL displayed significantly more positive resting membrane potentials when compared to neurons of the LGN and the NRT, while resting membrane potentials of LGN TC and NRT neurons were indistinguishable (Table 2). In addition to the stable resting membrane potential at around −75 mV, some NRT neurons of both strains displayed a prominent membrane potential bistability, as described previously (Blethyn et al., 2006; Fuentealba et al., 2005). This bistable behavior consisted of an oscillation between an “up state” and a “down state” (data not shown). The “up state” was usually initiated by a LTS crowned by a high frequency burst of action potentials, which gave way to tonic action potential generation (data not shown). The “up state” usually displayed membrane potentials in the range of −40 to −55 mV, while membrane potentials in the “down state” ranged from −50 to −65 mV. In some cases, rhythmic LTS generation was observed during the “down state” (not shown). In both strains, no intrinsic membrane potential rhythmicity was observed in LGN neurons. Some CL neurons of both strains displayed spontaneous LTS generation at sub-delta frequencies (data not shown).

Basic properties of the LTS of LGN, CL, and NRT neurons of WAG/Rij and ACI rats

Next, the basic features of the LTS in LGN TC, CL, and NRT neurons of WAG/Rij and ACI rats were examined. Via DC current injection, neurons were held at potentials around −60 mV, hyperpolarized to −100 mV for 800 ms to deinactivate I_T and repolarized to −60 mV (LGN TC and CL neurons) or to −55 mV (NRT neurons). A stronger DC current injection in NRT neurons was necessary to consistently evoke a LTS.

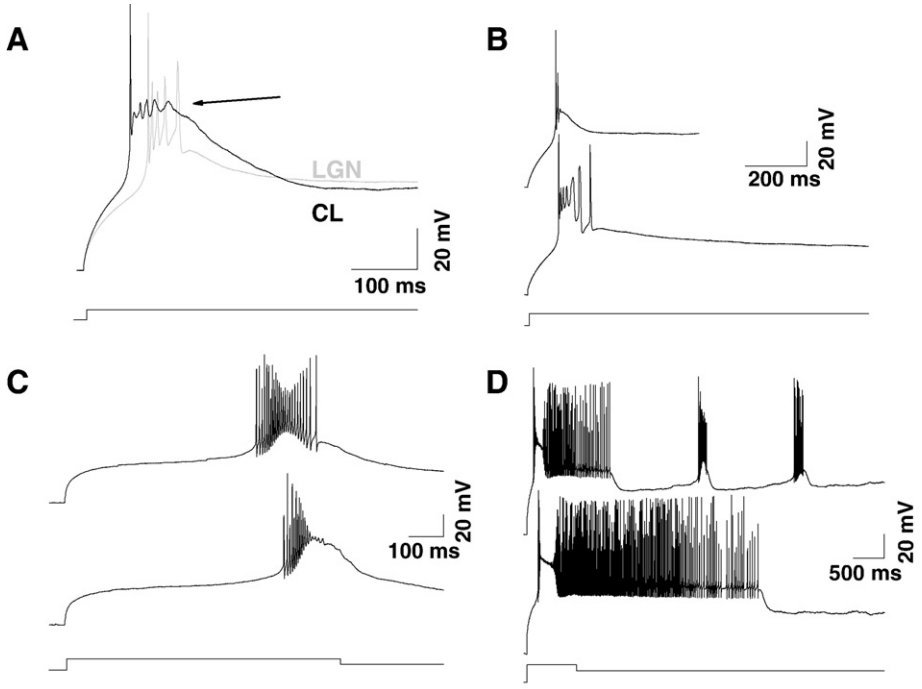

Fig. 5. The LTS of LGN TC, CL and NRT neurons. (A) Overlay of the LTS generated by a LGN TC neuron (grey trace) and a CL neuron (black trace). The LTS of CL neurons was of larger amplitude than the LTS of LGN TC neurons, but oftentimes generated only a single action potential. In case only a single action potential was generated, CL neurons often displayed a small amplitude membrane potential oscillation after the AP (indicated by the arrow). Both cells were taken from ACI rats. (B) Comparison of the LTS of two further LGN TC (upper panel) and CL (lower panel) neurons. The LTS of the CL neuron is of larger overall size and longer duration than the LTS of the LGN TC neuron. Note the increased width of the 5th and 6th action potentials of the CL neuron. The LTS of NRT neurons are displayed in C and D. (C) The LTS generated by NRT neurons oftentimes fell into one of two categories. Lower amplitude LTS evoked a large train of action potentials, displaying an accelerando/decelerando pattern (upper panel). The amplitudes of the action potentials generated in this manner were inversely correlated to the amplitude of the LTS. LTS of higher amplitude generated action potentials only during the initial rising phase (lower panel). Both recordings derive from the same ACI neuron. (D) In some NRT neurons, the LTS initiated upstate tonic action potential generation. Black lines below the recordings indicate DC current injection duration and magnitude. Both recordings derive from another ACI NRT neuron.

The shape of the LTS was similar in neurons recorded in the same nucleus of WAG/Rij and ACI rats. In comparison to CL neurons, the LTS of LGN TC neurons revealed smaller amplitudes and shorter durations, peaking at around 10–20 mV more negative values of the membrane potential (LGN TC: ~−40 mV; CL: ~−30 to −20 mV; Fig. 5A).

In the following, the number of LTS associated action potentials was investigated. On average, the LTS of a LGN TC neuron evoked 2.4±0.2 action potentials (n=25) in WAG/Rij and 2.4±0.2 action potentials (n=25) in ACI rats. The LTS of CL neurons oftentimes generated only a single action potential (15 of 26 ACI CL, 19 of 39 WAG/Rij CL) (Fig. 5A). In some of these cells, the initial action potential was followed by a transient depolarization of small amplitude reminiscent of an action potential, suggesting a depolarization block of I_{Na}, or a low amplitude membrane potential oscillation (arrow in Fig. 5A). On average, the LTS of a CL neuron evoked 2.3±0.2 action potentials (n=39) in WAG/Rij and 1.8±0.2 action potentials (n=26) in ACI rats. Furthermore, the LTS of CL neurons was usually slow to decline (Fig. 5B). The LTS of NRT neurons had a higher activation threshold and generated significantly higher numbers of action potentials than those of LGN TC and CL neurons. On average, the LTS of a NRT neuron elicited 9.9±1.7 action potentials (n=21) in WAG/Rij and 10.4±1.2 action potentials (n=39) in ACI rats (Table 2). Two main patterns of action potential generation were observed. Lower amplitude LTS evoked a large train of action potentials, displaying an accelerando/decelerando pattern (Fig. 5C, upper panel). The amplitudes of action potentials evoked in this manner were inversely correlated to the amplitude of the LTS, declining in amplitude from the beginning to the peak of the LTS and increasing in amplitude while the LTS declined. A LTS of higher amplitude generated action potentials only during the initial rising phase (Fig. 5C, lower panel). These action potentials also declined in amplitude as the LTS increased in amplitude. It is important to note, that both patterns of LTS associated action potential generation could be observed in the same neuron (Fig. 5C). In a subset of NRT neurons of both strains the LTS initialized “up state” tonic action potential generation (Fig. 5D).

In order to more clearly deduce whether variations in T-type Ca^{2+} currents cause alterations in LTS properties, we performed current-clamp experiments when Na^+–K^+ action potentials were blocked by 1 µM Tetrodotoxin (TTX, Figs. 6A–C). In the presence of TTX, the qualitative differences between nuclei were preserved in both strains. LGN TC neurons generated the smallest LTS (Fig. 6A), while CL (Fig. 6B) and NRT (Fig. 6C) neurons displayed LTS of higher amplitude and longer duration. The LTS of CL and LGN TC neurons were, except for the larger size in CL neurons, of quite similar shape. The LTS of NRT neurons differed by displaying slower rise and decay kinetics. No differences in the overall shape of the LTS were observed between WAG/Rij and ACI rats. The bistable behavior of a subset of NRT neurons was preserved in the presence of TTX (data not shown).

Since a close functional antagonism between I_T and the fast transient A-type K^+ current (I_A) has been described in LGN TC and NRT neurons (Meis et al., 1996; Pape et al., 1994) we further tried to isolate I_T generated LTS properties by blocking I_A with 4-Aminopyridine (4-AP, 5 mM) in combination with 1 µM TTX. Wash in of TTX and 4-AP enlarged the LTS and removed all action potentials (Figs. 6D–F). No qualitative differences were observed between strains. In LGN TC neurons, application of TTX and 4-AP increased the amplitude and prolonged the duration of the LTS (Fig. 6D, middle trace). In some neurons the initial LTS onset was followed by a second depolarizing rise of roughly equal slope (arrow in Fig. 6D, lower panel) probably representing a high threshold Ca^{2+} spike (HTS) (Hernandez-Cruz and Pape, 1989; Lo et al., 2002; Tennigkeit et al., 1998). It is important to note, that both forms could be observed in the same neuron, as shown

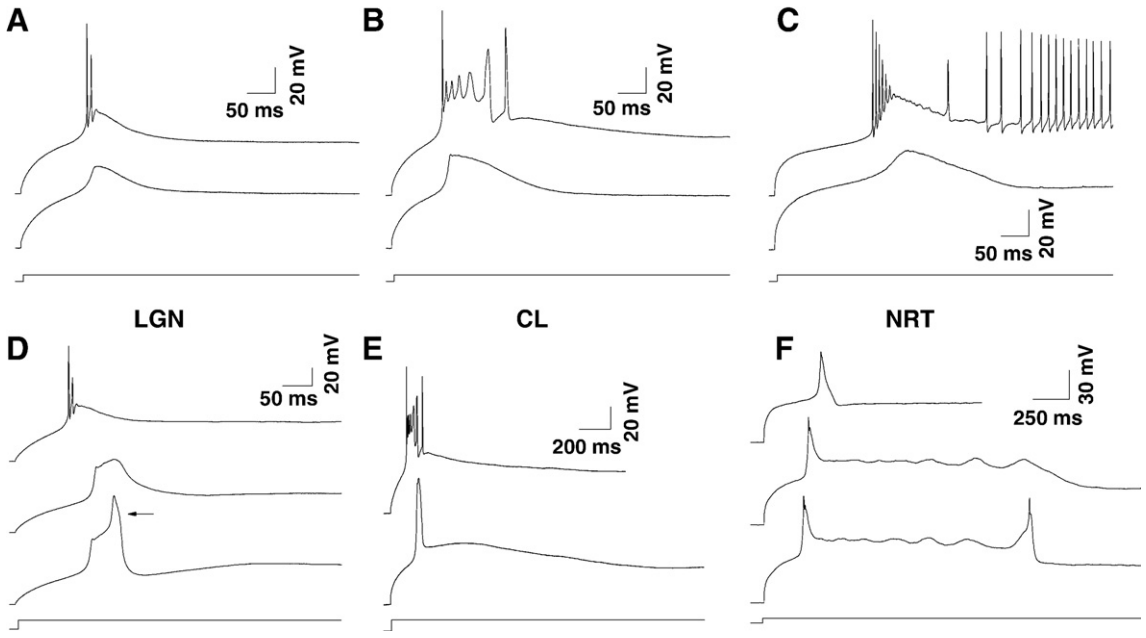

Fig. 6. LTS of LGN TC, CL, and NRT neurons under control conditions, in the presence of 1 μM TTX and under the influence of 1 μM TTX in combination with 5 mM 4-AP. Recordings in the presence of TTX are shown in A, B, and C. The effects of co-application of TTX and 4-AP are shown in D, E, and F. Neurons were held at −60 mV hyperpolarized to −100 mV for 800 ms before being stepped to ~−60 mV (LGN TC and CL) or ~−55 mV (NRT). The LTS of an LGN TC neuron is shown in A, the LTS of a CL neuron is shown in B, while C depicts the LTS of a NRT neuron. The upper panels show recordings under control conditions, the lower panels display recordings in the presence of TTX. (D) LTS of a LGN TC neuron under control conditions (upper panel) and in the presence of 1 μM TTX and 5 mM 4-AP (middle and lower panels). TTX and 4-AP transformed the LTS into a biphasic depolarization. The second depolarization could be of lower slope than the first (middle panel) or could be equally steep (arrow in the lower panel). The steep second depolarization shown in the lower panel was termed a "high threshold spike" (HTS), see text. (E) LTS of a CL neuron under control conditions (upper panel) and in the presence of 1 μM TTX and 5 mM 4-AP (lower panel). In CL neurons, drug application transformed the LTS into an initial depolarization, similar to the LTS of LGN TC neurons, and a slow depolarization. The slow depolarization could be of varying amplitude and duration. A prominent example of the slow depolarization is shown here. (F) After application of 1 μM TTX and 5 mM 4-AP the LTS of NRT neurons usually displayed one of three patterns: either the LTS was transformed into a single spike like depolarization (upper panel), which could be generated repetitively in some cells, or the LTS was transformed into a spike which was followed by a plateau depolarization (middle and lower panel panels). This plateau could or could not be terminated by a second LTS like depolarization in the same neuron. Black lines below the recordings indicate DC current injection duration and magnitude.

in Fig. 6D, and that the transition between the two phases could be more subtle than displayed. Similar to the LTS, the HTS behaved in a "nearly all or none manner" (Zhan et al., 1999), meaning either its complete presence or absence. Furthermore, the HTS was more readily observed when stronger/steeper depolarization was applied. In CL neurons, application of TTX and 4-AP transformed the LTS into a biphasic depolarization with an initial steep and transient component, similar to the LTS of LGN TC neurons, followed by a slow depolarization of varying duration and amplitude (Fig. 6E). In NRT neurons three patterns of LTS generation were observed after drug administration (Fig. 6F). In a subset of NRT neurons, the LTS was transformed into a single spike depolarization (Fig. 6F, upper panel), which could be generated repetitively in some cells. In other neurons, the LTS changed into a single spike followed by a plateau depolarization of varying duration, displaying low amplitude membrane potential oscillations (Fig. 6F, middle panel), reminiscent of the "up state" (see above). This plateau potential could sometimes be terminated by a second spike depolarization (Fig. 6F, lower panel).

Quantification of the LTS onset potential and the minimum LTS generating slope using current ramp stimulation

To correlate the I_T properties recorded under voltage clamp conditions with the LTS and to test the predictions of the mathematical model, we used current ramp stimulations. The experiments were designed to obtain a measure of the LTS onset potential and to investigate the stimulus intensity necessary for LTS generation.

Depolarizing current ramps were applied from a holding potential of −75 mV (Fig. 7). The slope of the current ramp induced depolarization was decreased until LTS generation ceased (Fig. 7). As has been observed previously, the LTS behaved in a "nearly all or none" manner (Zhan et al., 1999), meaning that it was present or absent with only very rarely displaying an intermediate size. The depolarization slope was decreased using two protocols: (1) Stimulation intensity was decreased, while the duration of the current ramps was kept constant (5 s). (2) Duration of the current ramps was increased, while the stimulation intensity was kept constant. Similar results were obtained with both paradigms. In the following only the results from the first paradigm using decreasing stimulation intensity will be presented. For quantification of LTS parameters, the LTS onset point was computed using the first derivative of the voltage trace. As described previously by Gutierrez et al. (2001), the LTS onset point was defined as the point where the slopes of 4 consecutive binned data points exceeded the baseline slope (see Experimental methods). Baseline slopes were obtained by a Gaussian fit of the differentiated membrane voltage prior to ramp stimulation (see Experimental methods). In a series of ramp stimulations with decreasing slopes the following parameters were obtained: (1) where applicable the voltage of the LTS onset point of the first LTS, (2) the minimum slope eliciting a LTS, and (3) the maximum slope eliciting no LTS, thereby setting the limits of a slope interval which includes the true minimal LTS generating slope. Application of depolarizing current ramps from −75 mV led to the generation of one or more LTS, followed by tonic action potential generation, if stimulation intensity was strong enough (Fig. 7). Decreasing the stimulation intensity first led to the disappearance of tonic action potentials, and subsequently to the disappearance of the LTS. In some cases ramps with shallow slope did not lead to LTS generation even though the threshold potential was reached. To account for this phenomenon the theoretical minimum slope necessary to reach the LTS onset potential was calculated for each neuron and the difference between this value and the minimal slope actually eliciting a LTS in the experiment was analyzed.

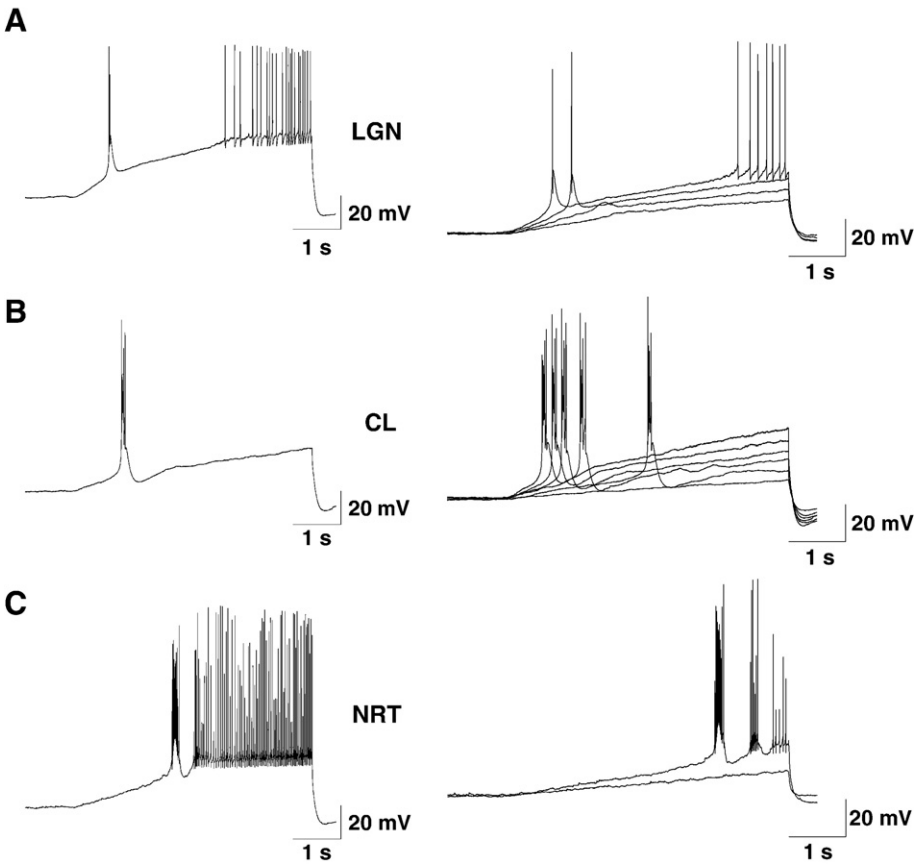

Fig. 7. LTS elicited via current ramp stimulation in LGN TC, CL, and NRT neurons. Single representative voltage traces are shown on the left side. The right side displays examples of the effects of stimulations of decreasing slope. Tonic action potentials disappeared first, followed by the disappearance of the LTS. Recordings from LGN TC neurons are shown in A, recordings from CL neurons are displayed in B, and recordings from NRT neurons are shown in C.

The LTS onset potentials varied little when elicited through current ramps of decreasing stimulus intensity in individual neurons. In both strains, NRT neurons displayed significantly more positive LTS onset potentials when compared to LGN TC and CL neurons (~−50 to −55 mV in NRT vs. ~−60 to −65 mV in LGN TC and CL; Fig. 8A, Table 2). LGN TC neurons displayed a slightly more depolarized LTS onset potential than CL neurons in WAG/Rij, while the opposite was found in ACI. The difference between LGN TC and CL neurons was significant in ACI. A comparison between WAG/Rij and ACI revealed ACI LGN TC neurons to generate the LTS at significantly more negative potentials when compared to WAG/Rij LGN TC neurons (Table 2).

In the following, the minimum depolarization slope leading to the generation of a LTS was analyzed. The minimal LTS generating slope varied between nuclei (Fig. 8B). In both strains, LGN TC neurons displayed the largest minimal LTS generating slope, while minimal LTS generating slopes in CL and NRT neurons were roughly similar (~8 to 11 mV/s in LGN TC vs. ~5 mV/s in CL and NRT, Table 2). In both strains, minimal LTS generating slopes were significantly higher in LGN TC neurons when compared to CL and NRT neurons, while differences between CL and NRT neurons were not significant. Furthermore, the minimal LTS generating slopes recorded in WAG/Rij LGN TC neurons were significantly smaller in comparison to the minimal LTS generating slopes recorded in ACI LGN TC neurons (Table 2). The relation between nuclei and strains observed for the maximum slope without LTS generation was similar to the results for the minimum slope generating a LTS (Fig. 8B).

Next, the difference between the calculated slope required for reaching the LTS onset potential and the measured minimal LTS generating slope was investigated. In both strains this difference was greatest in LGN TC neurons, with CL neurons displaying intermediate differences and minimal differences being observed in NRT neurons (Fig. 8C, Table 2). Within both strains, all differences between nuclei were significant. A comparison between strains revealed significant differences for LGN TC neurons (Table 2). Furthermore, these differences inversely correlated with the T-type Ca^{2+} current density within both strains, with cells displaying lower T-current density revealing a greater difference (Fig. 8D). This correlation was found to be nearly linear. It should be noted, however, that for neurons in the CL and NRT the higher T-current density in WAG/Rij compared to ACI did not translate into smaller differences between the minimal measured LTS generating slope and the minimal slope reaching the LTS onset potential.

In the following, LTS parameters were quantified in the presence of TTX (1 μM). An analysis of the LTS onset potentials and the minimal depolarization slopes leading to LTS generation during current ramp stimulation revealed no effect of TTX on the LTS onset potential in LGN TC and CL neurons of both strains (Figs. 9A, B). In contrast, the LTS onset potential of NRT neurons was depolarized by about 8 mV in both strains (from −52±3 to −44±1 mV in ACI, from −56±2 to −49±2 mV in WAG/Rij, in both strains $n=3$, Fig. 9C). Furthermore the minimal LTS generating slope was increased in all neurons (Figs. 9A–C; Table 2), indicating the contribution of persistent sodium currents (I_{NaP}) to the depolarization preceding an LTS. This effect was strongest in NRT neurons in both strains. Within both strains, LGN TC neurons, NRT neurons, and CL neurons revealed the greatest, intermediate, and smallest difference between the minimal LTS generating slope and the slope needed to cross the LTS onset potential, respectively. When strains were compared, neurons of WAG/Rij rats displayed smaller differences between the minimal LTS generating slope and the slope required to reach the LTS onset potential in all nuclei (Table 2).

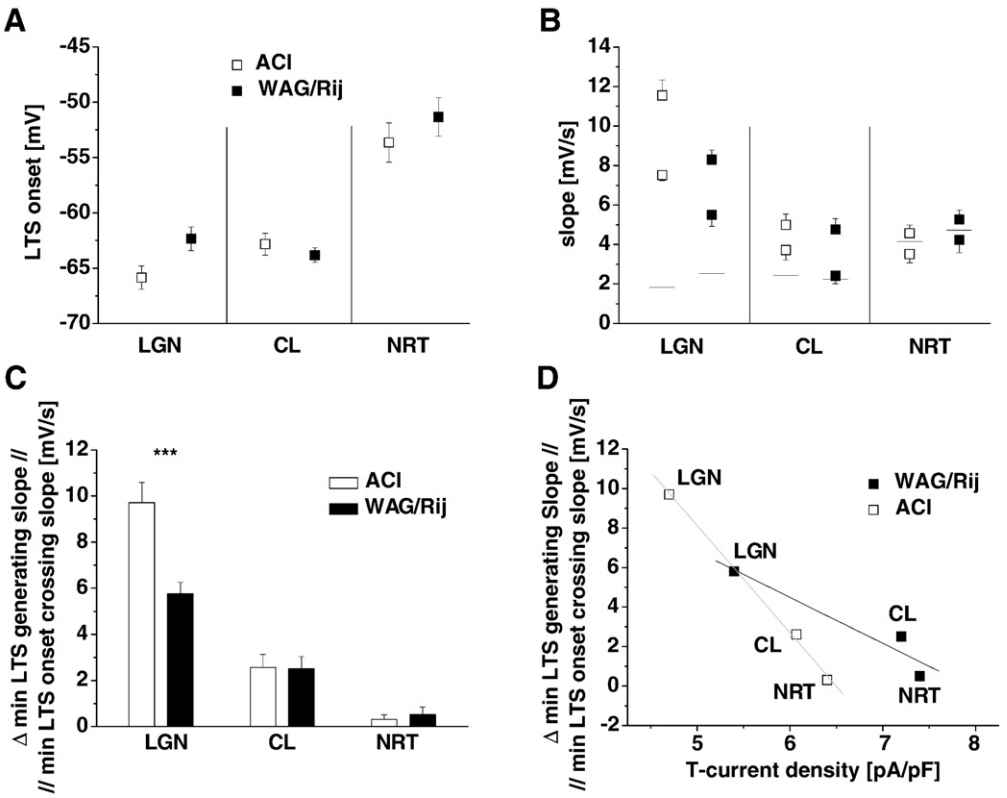

Fig. 8. Quantification of current ramp experiments. (A) The LTS onset potential of WAG/Rij (black) and ACI (white) LGN TC (left), CL (middle), and NRT (right) neurons. (B) Approximated minimal LTS generating slopes in WAG/Rij (black) and ACI (white) LGN TC (left), CL (middle), and NRT (right) neurons. For each population of neurons (e.g. WAG/Rij LGN TC, ACI LGN TC, WAG/Rij CL etc.) the upper square represents the mean minimal slope, which triggered a LTS in the experiment. The lower square represents the mean maximal slope, which did not trigger a LTS. The horizontal lines represent the mean minimum slope required to cross the LTS onset potential. (C) Difference between the minimal LTS generating slope and the minimal slope required to cross the LTS onset potential. (D) Correlation of the difference between the minimal LTS generating slope and the minimal slope required to cross the LTS onset potential and the T-type Ca^{2+} current density. The linear fit of the correlation for ACI is shown in grey ($r = 0.999$). The linear fit for WAG/Rij is depicted in black ($r = 0.958$).

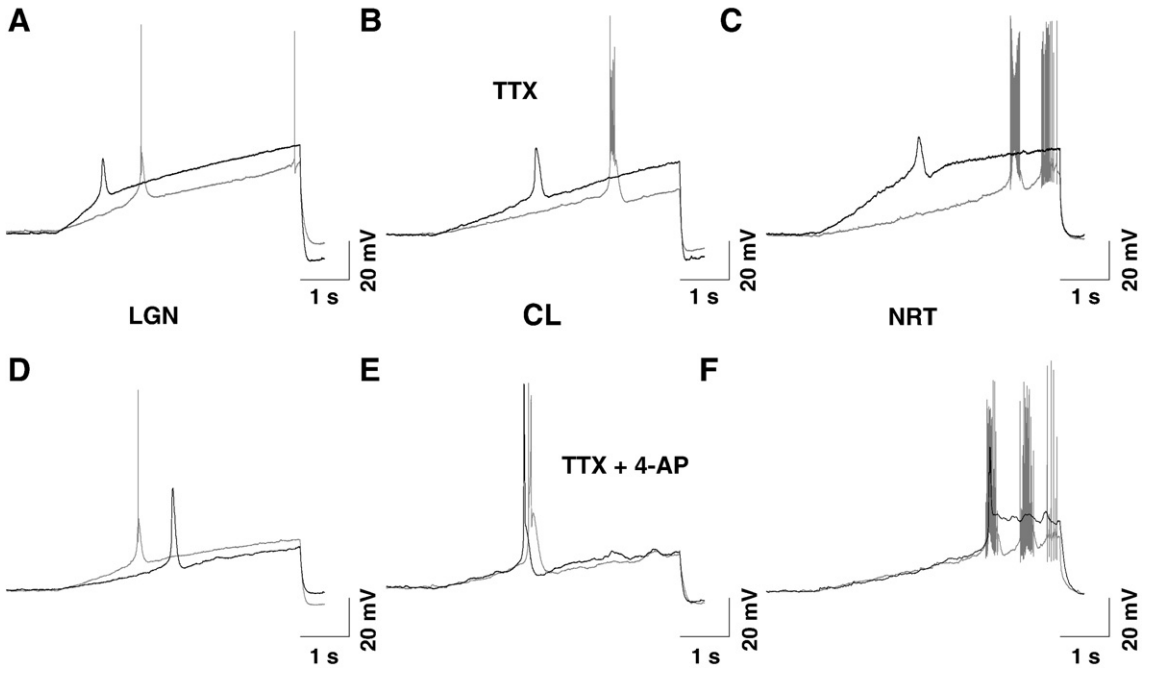

Fig. 9. Minimal LTS generating slopes during current ramp stimulation (from −75 mV, 5 s duration) under control conditions (grey traces) with the minimal LTS generating slopes in the presence of 1 μM TTX (A, B, C, black traces), or 1 μM TTX and 5 mM 4-AP (D, E, F, black traces). The LTS of LGN TC neurons are shown in (A) and (D), CL neurons are shown in (B) and (E), and NRT neurons are depicted in (C) and (F). Note the increased minimal LTS generating slope in all nuclei under the influence of 1 μM TTX (A, B, C). The combined effect of 1 μM TTX and 5 mM 4-AP reduced the minimal LTS generating slope in LGN TC neurons (D), while leaving the minimal LTS generating slopes of CL and NRT neurons basically unchanged (E, F).

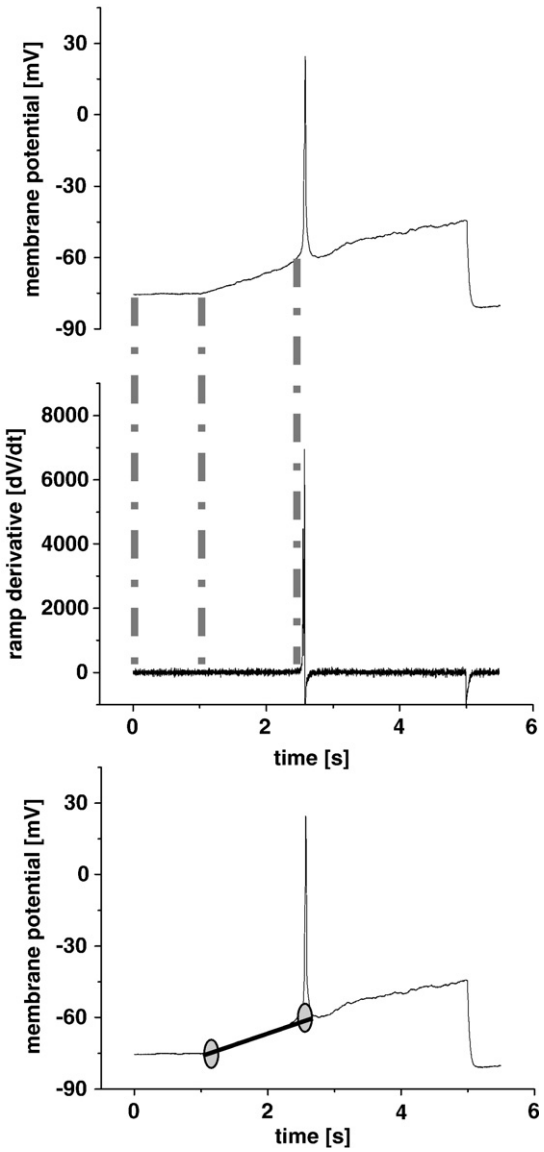

Fig. 10. The LTS onset point during current ramp stimulation. Prior to the beginning of the current ramp, a constant DC current was injected. This period is indicated by the left and middle lines connecting the upper 2 panels. The upper panel displays a voltage trace obtained using current ramp stimulation (in the presence of TTX and 4-AP) and the middle trace displays the differentiated voltage trace shown in the upper panel. The derivatives of the period of constant DC current injection were fitted with a Gaussian function. The LTS onset point was defined as the point were 4 consecutive derivatives exceeded the upper 95% confidence limit of the Gaussian fit of the baseline period and is indicated by the right line connecting the upper 2 panels. Subsequently, the voltage trace between the beginning of current ramp stimulation (middle line connecting the upper two panels, left ellipse in the lower panel) and the LTS onset point (right line connecting upper two panels and right ellipse in the lower panel) was fit with a linear equation (line in the lower panel), yielding the depolarization slope. See also Gutierrez et al., 2001.

In a next step TTX and 4-AP (1 μM and 5 mM, respectively) were co-applied to thalamic slices. The LTS onset potential was hyperpolarized to −66±1 mV (n=11) in ACI CL, with no changes observed in the other two nuclei or in WAG/Rij. The minimal slope leading to LTS generation did not change much in NRT neurons of both strains (Fig. 9F), but was decreased in LGN TC and CL neurons, although this effect was small in the CL (Figs. 9D, E; Table 2). When strains were compared, neurons of WAG/Rij rats displayed smaller differences between the minimal LTS generating slope and the slope required to reach the LTS onset potential in all nuclei (Table 2).

Discussion

The present study investigated the expression of T-channel coding mRNA, as well as the I_T, and the LTS in three functionally distinct thalamic nuclei of WAG/Rij and ACI rats. Results show that distinct T-channel expression patterns translate into different T-currents, which give rise to different LTS. While a good correlation between T-channel coding mRNA and I_T was observed, the correlation between I_T and the LTS was more complex, suggesting the contribution of additional factors. When WAG/Rij and ACI rats are compared, this study indicates that the LTS is similar in both strains, despite quantitative differences in I_T. For LGN TC neurons, a population of prototypical specific thalamocortical relay neurons, an increased robustness of LTS generation was observed in WAG/Rij. If this finding extends to other populations of TC neurons, the increased robustness of burst firing could be implicated in the generation and/or maintenance of SWD, which is thought to be accompanied by thalamic burst mode transmission.

Relation of tissue mRNA expression and neuronal subpopulations in the LGN, CL, and NRT

In agreement with previous studies (Talley et al., 1999) and the results of RT-PCR experiments on isolated neurons (Broicher et al., 2007a), the thalamic relay nuclei of WAG/Rij and ACI rats primarily expressed the α1G isoform, while the NRT was found to primarily express the α1H and α1I isoforms. In addition to α1G, expression of the α1I isoform was detected in the LGN and CL. While α1I expression can be attributed to local circuit interneurons in the LGN (Broicher et al., 2007a), the cell type specific attribution of expression signals in the CL is less clear. Electrophysiological evidence as well as anatomical tracing studies indicate a uniform population of neurons displaying similar electrophysiological characteristics as well as homogeneous axonal projections (Deschenes et al., 1996; Lacey et al., 2007; Van der Werf et al., 2002; Yasukawa et al., 2004). It is thus reasonable to assume that both splice variations of the α1G isoform as well as the α1I isoform are present in typical CL neurons.

In case of the reticular nucleus, a functional distinction between bursting and non-bursting neurons, which either do or do not posses a T-type Ca^{2+} conductance is proposed by some authors (Lee et al., 2007). Furthermore, a subpopulation of NRT neurons has been described to display a membrane potential bistability (Blethyn et al., 2006; Fuentealba et al., 2005). All NRT neurons recorded during the course of this study possessed a T-type Ca^{2+} conductance or a LTS, while a subpopulation of NRT neurons displayed membrane potential bistability. There was no obvious correlation between the presence and absence of bistable behavior and LTS properties or other cellular parameters investigated in this study. The expression α1H and α1I observed in NRT tissue samples is thus interpreted to correspond to an expression of both isoforms in typical NRT neurons.

Correlation of T-channel coding mRNA and I_T in neurons of the LGN, CL, and NRT

The relation of the T-type Ca^{2+} current voltage dependencies of activation and inactivation, as well as the relation of the activation and inactivation kinetics between LGN TC, CL, and NRT neurons within both strains matched the predictions from studies on cloned channels (Chemin et al., 2001, 2002; Emerick et al., 2006): (i) As has been shown before (Broicher et al., 2007a), LGN TC neurons solely express the α1G-a isoform. This correlates well with an I_T of comparatively negative voltage dependency and fast kinetics. (ii) Neurons of the CL displayed T-type Ca^{2+} currents of intermediate voltage dependency and kinetics. These neurons expressed both the α1G-a, and the α1G-bc splice variants, as well as the α1I isoform. The I_T voltage dependency of activation of CL neurons can be

explained by the presence of the α1G-bc splice variation and the α1I isoform or by a combination of both (Chemin et al., 2001, 2002; Emerick et al., 2006). Furthermore, currents carried by α1G (irrespective of splice variation) display considerably faster current kinetics than currents carried by α1I, while the differences in I_T kinetics between α1G-a and α1G-bc splice variations are rather moderate by comparison (Chemin et al., 2001, 2002; Emerick et al., 2006). Together with the current properties of LGN TC (primarily α1G-a) and NRT (primarily α1I) neurons and the higher expression of α1G than α1I (~16 times, under the assumption of similar primer/probe efficiency), these data argue for a stronger contribution of α1G-bc than α1I in CL neurons. (iii) In NRT neurons, the slow kinetics of activation and inactivation argue for a stronger influence of the α1I isoform than the α1H isoform on the whole-cell T-type Ca^{2+} current. Further support of this notion comes from experiments investigating the deactivation kinetics of I_T. Here, the I_T of NRT neurons displayed faster kinetics than the I_T of LGN TC and CL neurons (T.B. and T.B., unpublished observations), which correlates well with the fast deactivation kinetics of α1I carried currents in heterologous expression systems. This interpretation is further supported by the ~2.5-times higher expression of α1I coding mRNA in comparison to α1H coding mRNA (under the assumption of similar primer/probe efficiency) in the NRT.

Correlation of T-channel coding mRNA and I_T in neurons of WAG/Rij and ACI

Neurons recorded in all three nuclei of WAG/Rij rats displayed increased I_T densities when compared to ACI. This finding is in good agreement with the increased expression of T-channel coding mRNA in WAG/Rij. Surprisingly, and in contrast to previous recordings performed on isolated neurons of the LGN (Broicher et al., 2007a), I_T voltage dependencies were different between neurons of the same nucleus recorded in WAG/Rij and ACI in brain slice preparations. LGN TC neurons and CL neurons of WAG/Rij displayed more negative I_T voltage dependencies in comparison to ACI, while NRT neurons of WAG/Rij were found to display slightly more positive I_T voltage dependencies. The molecular data suggests that this difference is neither due to differences in isoform expression or alternative splicing of exons 25/26, nor caused by a different ratio of isoform quantities. It should be kept in mind however, that alternative splicing in other regions of the pre-mRNA may underlie the observed differences. A previously described mathematical model, investigating the effects of different somatodendritic T-type Ca^{2+} channel distributions on the somatically recorded I_T voltage dependency, offers a possible explanation for this unexpected finding (Broicher et al., 2007a). The model has shown that an increased distal dendritic T-channel localization results in a negative shift of the somatically recorded T-type Ca^{2+} current voltage dependency. Possibly, there is a difference in the localization of T-type Ca^{2+} channels between thalamocortical neurons of WAG/Rij and ACI. This differential channel distribution could cause a difference in the somatically recorded T-type Ca^{2+} current voltage dependency in brain slice preparations, but would be undetectable in acutely isolated neurons, which lack most of their distal dendrites (Destexhe et al., 1998; Zhang et al., 2002). It has been shown that the synaptic terminals of inhibitory NRT and excitatory cortical afferents are located on the distal dendrites of TC neurons (Sherman and Guillery, 2006). An increased T-channel density in this region may thus augment TC neuron burst firing and contribute to SWD in WAG/Rij rats (Budde et al., 2006).

General correlation of I_T with the LTS in LGN TC, CL, and NRT neurons of WAG/Rij and ACI rats

The most straight forward correlation of I_T and the LTS could be established for the relationship between current density and the size of the LTS. NRT and CL neurons displayed LTS of higher amplitude and longer duration than LGN TC neurons. Another central finding of the present study is that the LTS recorded in LGN TC, CL, and NRT neurons are qualitatively different, while the LTS recorded in the same nucleus of WAG/Rij and ACI rats are qualitatively similar. Although differences in T-type Ca^{2+} currents can be expected to be the primary cause for differences in the LTS, a number of other factors influence shape and amplitude of the LTS. These factors include channel distribution, cell geometry, K^+ currents activating below threshold (I_A), Ca^{2+}-dependent K^+ currents (I_{KCa}), the persistent sodium current (I_{NaP}), and the hyperpolarization-activated cation current (I_h) (Broicher et al., 2007a; Destexhe et al., 1998; Mainen and Sejnowski, 1996; van Ooyen et al., 2002; Williams and Stuart, 2000; Zhang et al., 2002).

In an attempt to exclude some of these complicating factors we used the Na^+ current blocker TTX. Indeed this maneuver more clearly dissected the shape of the LTS. While the mainly α1G-based Ca^{2+} currents in LGN TC and CL neurons generated spikes of similar shape (with LTS amplitudes being higher in CL neurons), the α1I/α1H-based I_T of NRT neurons generated an LTS of slower rise and decay kinetics and thus longer duration. Although TTX was helpful for the interpretation of step responses, it created additional complicating factors for the analysis of ramp responses since blocking of I_{NaP} altered the steepness of the ramp. The additional block of I_A by 4-AP allowed the occurrence of HTS possibly due to the activation of high voltage-activated (HVA) Ca^{2+} channels, distal dendritic T-type Ca^{2+} channels, or a combination of both (Crunelli et al., 2006; Hernandez-Cruz and Pape, 1989; Lo et al., 2002; Tennigkeit et al., 1998) thereby masking the exact LTS shape. The HTS was only observed in LGN TC and CL neurons, but never in NRT neurons. The rising phase of the LTS in TTX/4-AP was rapid in all cell types, thereby demonstrating the influence of 4-AP sensitive currents. These findings demonstrate that a clear correlation between T-type Ca^{2+} current properties and LTS is difficult to achieve.

Correlation of I_T voltage dependency and the LTS in neurons of the LGN, CL, and NRT of WAG/Rij and ACI rats

With keeping the above mentioned problems in mind the LTS onset potential was used in an attempt to find a correlation with the voltage dependency of I_T activation. The LTS onset potential was approximated by an algorithm using the increasing voltage slopes (dV/dt) during LTS generation. Computational modeling predicted the LTS onset potential to correlate with the voltage dependency of I_T activation. Overall this suggestion was corroborated by the experimental data retrieved from both strains. Only the LTS onset potential of WAG/Rij LGN TC neurons seems too depolarized with respect to the V_h value of I_T activation. A possible explanation for this finding comes from the fact that the LTS is shaped by I_h (Pape, 1996; Ying et al., 2006). Since it has been shown that the voltage dependency of I_h is shifted to more hyperpolarized potentials in WAG/Rij compared to ACI LGN TC neurons, the weaker I_h-induced overshoot may contribute to the more depolarized LTS onset in WAG/Rij (Budde et al., 2005). While there seems to be no influence of Na^+ currents on the LTS onset potential in LGN TC and CL neurons, a strong depolarization was observed in NRT neurons. Interestingly, the depolarization of the LTS onset potential was not observed after wash in of TTX/4-AP, pointing to a scenario where TTX and 4-AP sensitive components exert equal, functionally antagonistic influences on the LTS onset potential in NRT neurons.

Correlation of T-current density and the LTS in neurons of the LGN, CL, and NRT of WAG/Rij and ACI rats

The number of LTS associated action potentials was predicted to be influenced by the T-type Ca^{2+} current density by the mathematical model. In the model, an increased I_T density resulted in an increased number of action potentials. Despite the increased I_T density in WAG/Rij no differences in the number of LTS associated action potentials

were found between WAG/Rij and ACI neurons of the same type, indicating that single bursts of individual thalamic neurons are unchanged in WAG/Rij rats.

Furthermore, a clear correlation of the T-type Ca^{2+} current density and the depolarizing slopes required to elicit a LTS was observed in ramp stimulation experiments. The comparison between the difference of the minimal slope required to reach the LTS onset potential and the minimal slope eliciting a LTS revealed a nearly linear correlation with the T-current density within both strains. Applied to an *in vivo* situation, this finding suggests that weaker depolarizations from hyperpolarized membrane potentials are sufficient to elicit a LTS in CL and NRT neurons in comparison to LGN TC neurons, provided that the potential for the regenerative activation process is reached.

Wash in of TTX increased the minimal LTS generating slopes as well as the differences between the minimal LTS generating slopes and the minimal slope required to cross the LTS onset potential in all neurons tested, indicating a contribution of the persistent sodium current. When TTX was co-applied with 4-AP, LTS generating slopes decreased in LGN TC and CL neurons (although this effect was very small in ACI CL neurons), but not in NRT neurons. Together with the effect of TTX on the LTS onset potential in NRT these data point to a different contribution of TTX and 4-AP sensitive conductances in relay (LGN TC and CL) and NRT neurons.

When strains were compared, the correlation between the T-current density and the LTS generating slopes was less clear. Here, significant differences were found between LGN TC, but not between CL or NRT neurons of WAG/Rij and ACI rats. Still, this finding indicates a more robust LTS generation in a specific thalamic relay nucleus of epileptic WAG/Rij rats. An increased likelihood of burst generation in WAG/Rij rats is in good agreement with an absence epilepsy phenotype, as thalamic burst mode transmission is thought to coincide with SWDs. Possibly, the lack of difference between CL and NRT neurons of WAG/Rij and ACI rats is due to the very small differences between the LTS onset potential crossing slope and the minimal LTS generating slope observed in these neurons. It cannot be excluded that our detection method was insufficient to resolve subtle differences between these two neuronal populations. Under the influence of TTX and TTX/4-AP, LTS generating slopes were smaller in WAG/Rij when compared to ACI. This finding fits well with the increased I_T density observed in the WAG/Rij strain.

Comparison to other models of absence epilepsy

Abnormalities in T-type Ca^{2+} channels have been implicated in the rodent and human absence phenotype for a long time and an augmentation of thalamic I_T seems to be a general motive in rodent models of absence epilepsy (Budde et al., 2006; Crunelli and Leresche, 2002; Pinault and O'Brien, 2007). An increased I_T has been observed in TC neurons of several mutant mouse strains (tottering, lethargic, stargazer, coloboma) and α1A knock-out mice displaying an absence phenotype with ataxia (Song et al., 2004; Zhang et al., 2002, 2004). Crossbreeding α1G knock-out mice with these mutant mice abolishes SWD in the progeny (Song et al., 2004). Studies in Genetic Absence Epilepsy Rats from Strasbourg (GAERS) revealed an increased I_T and expression of α1H mRNA in the NRT of pre-seizure and adult rats (Kuisle et al., 2006; Talley et al., 2000; Tsakiridou et al., 1995), thereby indicating the importance of burst activity in the NRT in the absence phenotype. This view is further supported by the finding that SWDs in mice are unaltered with a genetically induced 25% reduction of α1G carried I_T, which is presumably restricted to thalamic relay and cortical neurons, but probably leaves the α1H and α1I carried I_T of NRT neurons unchanged (Song et al., 2004). Therefore, an enhanced I_T in distinct thalamic regions might be tightly linked to SWD expression.

Experimental methods

The experimental procedures were applied on rats of both strains (WAG/Rij and ACI) in an identical manner. All experiments were performed on rats of both sexes. Unless stated otherwise, all chemicals were obtained from Sigma (Sigma-Aldrich, Germany). All animal procedures were approved by the local authorities.

Preparation of brain slices for electrophysiology

For patch-clamp experiments on brain slices, rats (postnatal day 15 to 25, P15 to P25) were deeply anesthetized with isoflurane (Forene, Abbott) and decapitated. Brains were removed and placed in cold, oxygenated sodium free artificial cerebrospinal fluid (ACSF) containing (mM): sucrose, 210; PIPES, 20; KCl, 2.4; $MgCl_2$, 10; $CaCl_2$, 0.5; dextrose, 10; pH 7.25 with NaOH. The cerebellum and the anterior third of the brain were removed before the brain was glued on the rostral side onto a vibratome (Model 1000, Ted Pella, Redding, CA), doused with cold sodium free, high sucrose ACSF and cut into coronal slices (300 µm). Brain slices containing the LGN and the CL were transferred into a holding chamber. For recordings in the NRT, horizontal brain slices were used. These were obtained by removing the brain as described above, and gluing the ventral side onto a vibratome. Three hundred µm thick horizontal slices were obtained and transferred into a holding chamber. The holding chamber was filled with identical solutions for coronal and horizontal slices, which were composed of (mM): $CaCl_2$, 3; KCl, 2.5; NaCl, 125; $MgSO_4$, 4; NaH_2PO_4, 1.25; $NaHCO_3$, 22; dextrose, 10; pH ~7.4, gassed with carbogen. Slices were heated for 20 min to 30 °C before being cooled to room temperature, and allowed to rest for 60 to 90 min.

Electrophysiology

Whole-cell recordings in brain slice preparations were done using glass pipettes (GC150T-10, Clark Electromedical Instruments, Pangbourne, UK) connected to an EPC-10 amplifier (HEKA Elektronik, Friedland, Germany). Pulse software (HEKA) was used for stimulus application and the recording of data. Electrode resistances ranged from 1.8 to 2.5 MΩ. Input resistances ranged from 200 to 800 MΩ, while series resistances ranged from 5 to 15 MΩ. All recordings were performed at room temperature. The following recording solutions were used to isolate Ca^{2+} currents in voltage clamp experiments: i) Extracellular solution (mM): $CaCl_2$, 1.5; KCl, 2.5; NaCl, 120; $MgSO_4$, 2; NaH_2PO_4, 1.25; HEPES, 30; dextrose, 10; 4-AP, 2; TEA, 5; TTX, 0.0005; pH 7.24 with NaOH. ii) Intracellular solution (mM): Cs-gluconate, 80; Cs_3-citrate, 10; NaCl, 10; HEPES, 10; EGTA, 11; $CaCl_2$, 1; $MgCl_2$, 1; KCl, 1; TEA-Cl, 15; QX-314, 1 mg/ml internal solution; Biocytin, 3 mg/ml internal solution; Mg-ATP, 3; Na_2-GTP, 0.5; phosphocreatine, 15; pH 7.25 with CsOH; ~290 mOsm. For current-clamp experiments in brain slice preparations the following recording solutions were used: i) Extracellular solution (mM): $CaCl_2$, 1.5; KCl, 2.5; NaCl, 120; $MgSO_4$, 2; NaH_2PO_4, 1.25; HEPES, 30; dextrose, 10; pH 7.24 with NaOH; ~300 mOsm. ii) Intracellular solution (mM): $CaCl_2$, 0.5; NaCl, 10; $MgCl_2$, 1; HEPES, 10; K-BAPTA, 5; K-gluconate, 95; K_3-citrate, 20; phosphocreatine, 15; Na_2-GTP, 0.5; Mg-ATP, 3; Biocytin, 3 mg/ml internal solution; pH 7.24 with KOH; ~290 mOsm.

Analysis of electrophysiological data

All current traces of voltage clamp experiments were subjected to off-line subtraction of the linear leak according to Ohm's law, using custom made software (Patch by Bernd Letz, HEKA).

The maximum T-type Ca^{2+} current amplitude observed during the steady-state activation protocol was taken as the maximum T-current

amplitude for each individual neuron. This amplitude was used for the calculation of T-current density.

The inactivation time constant of the T-type Ca^{2+} current was obtained by fitting a mono-exponential decay function to the inactivating part of the T-current trace using PulseFit software. The function had the following form:

$$Y = A + I_{max} e^{-x/t} \quad (1)$$

Numerical analysis of current-clamp data was done using MATLAB® software (MathWorks). For analysis of current ramps, data were binned (9.8 ms intervals) and differentiated. To approximate the beginning of the LTS we adapted a method described by Gutierrez et al. (2001). Briefly, the recorded voltage prior to ramp stimulation (baseline) was differentiated and fitted with a Gaussian function (Fig. 10). The LTS onset point was defined as the first point after which 4 consecutive slopes of binned data exceeded the upper 95% confidence limit of the Gaussian fit of the baseline (Fig. 10) (Gutierrez et al., 2001). Subsequently, the data between the onset point of ramp stimulation and the onset of the LTS were fitted with a linear equation. The voltage of the LTS onset point, and the slope between the beginning of the stimulation and the LTS onset point were used for analysis. In case of ramp stimulations without LTS generation, the entire ramp was fitted with a linear function.

Laser capturing of thalamic tissue

All solutions used during the preparation of slices for laser capturing were prepared with DEPC treated water and RNAse free components. Rat brains (P18–28) were removed, embedded in tissue freezing medium (Tissue-Tek, Science Services, Munich, Germany) and stored at −80 °C for further processing. Later, brains were placed into a cryo-microtome (−12 to −16 °C) and allowed to equilibrate for ~1 h. Then, brains were cut into 16 µm thick slices and placed onto Poly-L-Lysin (0.05%) treated membrane coated object slides (PALM MembraneSlides, P.A.L.M. Microlaser Technologies AG, Bernried, Germany). Afterwards, the brain slices were stained with Hematoxylin and Eosin (Hematoxylin 1 min; 3× wash in DEPC-H_2O for 1, 2, and 3 min; Eosin 30 s; increasing ethanol series, 50%, 70%, 100% for 3 min each; air dried at room temperature) and placed under an inverted laser capture microscope (P.A.L.M. Microlaser Technologies AG). The LGN, CL, and NRT were shot into mineral oil filled caps of laboratory tubes and frozen in liquid nitrogen to be subjected to RT-PCR procedures.

RT-PCR procedures

Quantitative RT-PCR analysis was performed on LGN, CL, and NRT tissue yielded through laser capturing. The mRNA of laser captured tissue was transcribed into cDNA using oligo$(dT)_{18}$ primers (Roche, Germany) and the Sensiscript RT Kit (Quiagen, Hilden, Germany). The hybridization primer/probe assays for real-time PCR detection were purchased from Applied Biosystems. The following intron spanning assay-on-demand probes were used: α1G: Rn0058105_m1; α1H: Rn01460351_g1; α1I: Rn00571684_m1; β_2-microglobulin: Rn00560865_m1. Real-time PCR was performed using the TaqMan universal PCR Master Mix (Applied Biosystems) and the ABI Prism 7000 Sequence Detection System (Applied Biosystems); PCR program was: 2 min at 50 °C, 10 min at 95 °C, 50 cycles: 15 s at 95 °C and 1 min at 60 °C. Results were analyzed with the ABI Prism 7000 SDS software. The efficiency of real-time primer/probes was nearly identical. Quantification was done using the comparative C_T or $\Delta\Delta C_T$ method as described earlier (Budde et al., 2005). Non-quantitative RT-PCR for detection of splice variations of the CACNA1G transcript was performed on CL tissue samples obtained through laser capturing (Broicher et al., 2007a). GAPDH expression was checked as a positive control. The PCR protocol for GAPDH amplification was: 3 min 94 °C; 50 cycles (30 s 94 °C, 1 min 61 °C, 1 min 72 °C); 7 min 72 °C; ∞ 4 °C. Primer sequences for GAPDH (nucleotides 789–1028, accession no. NM017008) were: forward, 5′-TGATGACATCAAGAAGGTGGTGAA-3′; reverse, 5′-TCCTTGGAGGCCATG-TAGGCCAT-3′. Amplification of the exon 25, 26 region was done using a nested PCR approach. The PCR protocol for the multiplex step was: 3 min 94 °C; 50 cycles (30 s 94 °C, 1 min 62 °C, 1 min 72 °C); 7 min 72 °C; ∞ 4 °C. The PCR protocol for the nested step was: 3 min 94 °C; 35 cycles (30 s 94 °C, 1 min 64 °C, 1 min 72 °C); 7 min 72 °C; ∞ 4 °C. Primer sequences for the multiplex step were (nucleotides 4557–5361; accession no. AF290212): forward, 5′-CAGCAGCCCATCATGAACCAC-AAC-3′; reverse, 5′-GCCGACCCAAGCCCTCACAAG-3′. Primer sequences for the nested step were (nucleotides 4709–5034; accession no. AF290212): forward, 5′-GCGGCGTGAGGAGAAGCGACTAC-3′; reverse, 5′-CCTGGAAGAAACGGCGGAAGC-3′. For all non-quantitative PCRs the Taq DNA Polymerase (5 U/µl, Quiagen) was used.

Computational modeling

For simulations on the effects of different T-current characteristics on the LTS, a single compartment TC neuron model was used, as described previously (Hines and Carnevale, 2001; Meuth et al., 2006). The model was based on the mathematical description of $I_{K\ leak}$, $I_{Na\ leak}$, I_L, I_T, $I_{Na\ HH}$, I_{NaP}, $I_{K\ HH}$, I_A, and I_{KCa}. Neuronal membrane potential was described by the following equation: $C_M(dV/dt) = -I_M + I_{inject}$. I_M is the sum of all membrane currents, I_{inject} is the injected current, and C_M is the membrane capacitance. The model was capable of generating action potentials in both burst and tonic transmission modes. Simulations were carried out at 35 °C using the NEURON simulation environment (Hines and Carnevale, 2001).

Acknowledgments

The authors would like to thank A. Jahn, A. Ritter, and R. Ziegler for their excellent technical assistance. This work was supported by grants from DFG (Pa 336/17-1 to H-C.P. and Bu 1019/8-1 to T. Budde), MPG (Research Award to H-C.P.), IZKF (Bud 3/005/07 to T. Budde), and IMF (Bu 120 501 to T. Budde). T. Broicher was a fellow of the Boehringer Ingelheim Foundation.

References

Anderson, M.P., Mochizuki, T., Xie, J., Fischler, W., Manger, J.P., Talley, E.M., Scammell, T.E., Tonegawa, S., 2005. Thalamic Cav3.1 T-type Ca2+ channel plays a crucial role in stabilizing sleep. Proc. Natl. Acad. Sci. U. S. A. 102, 1743–1748.

Avoli, M., Rogawski, M.A., Avanzini, G., 2001. Generalized epileptic disorders: an update. Epilepsia 42, 445–457.

Blethyn, K.L., Hughes, S.W., Toth, T.I., Cope, D.W., Crunelli, V., 2006. Neuronal basis of the slow (<1 Hz) oscillation in neurons of the nucleus reticularis thalami in vitro. J. Neurosci. 26, 2474–2486.

Broicher, T., Kanyshkova, T., Landgraf, P., Rankovic, V., Meuth, P., Meuth, S.G., Pape, H.C., Budde, T., 2007a. Specific expression of low-voltage-activated calcium channel isoforms and splice variants in thalamic local circuit interneurons. Mol. Cell. Neurosci. 36, 132–145.

Broicher, T., Seidenbecher, T., Meuth, P., Munsch, T., Meuth, S.G., Kanyshkova, T., Pape, H.C., Budde, T., 2007b. T-current related effects of antiepileptic drugs and a Ca2+ channel antagonist on thalamic relay and local circuit interneurons in a rat model of absence epilepsy. Neuropharmacology 53, 431–446.

Budde, T., Caputi, L., Kanyshkova, T., Staak, R., Abrahamczik, C., Munsch, T., Pape, H.C., 2005. Impaired regulation of thalamic pacemaker channels through an imbalance of subunit expression in absence epilepsy. J. Neurosci. 25, 9871–9882.

Budde, T., Pape, H.-C., Kumar, S.S., Huguenard, J.R., 2006. Thalamic, thalamo-cortical, and cortico-cortical models of epilepsy with an emphasis on absence seizures. In: Pitkänen, A., Schwartzkroin, P.A., Moshé, S.L. (Eds.), Models of Seizures and Epilepsy. Elsevier, Amsterdam, pp. 73–88.

Chemin, J., Monteil, A., Bourinet, E., Nargeot, J., Lory, P., 2001. Alternatively spliced alpha (1G) (Ca(V)3.1) intracellular loops promote specific T-type Ca(2+) channel gating properties. Biophys. J. 80, 1238–1250.

Chemin, J., Monteil, A., Perez-Reyes, E., Bourinet, E., Nargeot, J., Lory, P., 2002. Specific contribution of human T-type calcium channel isotypes (alpha(1G), alpha(1H) and alpha(1I)) to neuronal excitability. J. Physiol. 540, 3–14.

Coenen, A.M., Van Luijtelaar, E.L., 2003. Genetic animal models for absence epilepsy: a review of the WAG/Rij strain of rats. Behav. Genet. 33, 635–655.

Coulter, D.A., Huguenard, J.R., Prince, D.A., 1989a. Characterization of ethosuximide reduction of low-threshold calcium current in thalamic neurons. Ann. Neurol. 25, 582–593.

Coulter, D.A., Huguenard, J.R., Prince, D.A., 1989b. Specific petit mal anticonvulsants reduce calcium currents in thalamic neurons. Neurosci. Lett. 98, 74–78.
Crunelli, V., Leresche, N., 2002. Childhood absence epilepsy: genes, channels, neurons and networks. Nat. Rev. Neurosci. 3, 371–382.
Crunelli, V., Cope, D.W., Hughes, S.W., 2006. Thalamic T-type Ca2+ channels and NREM sleep. Cell. Calcium. 40, 175–190.
Deschenes, M., Bourassa, J., Parent, A., 1996. Striatal and cortical projections of single neurons from the central lateral thalamic nucleus in the rat. Neuroscience 72, 679–687.
Destexhe, A., Neubig, M., Ulrich, D., Huguenard, J., 1998. Dendritic low-threshold calcium currents in thalamic relay cells. J. Neurosci. 18, 3574–3588.
Emerick, M.C., Stein, R., Kunze, R., McNulty, M.M., Regan, M.R., Hanck, D.A., Agnew, W.S., 2006. Profiling the array of Ca(v)3.1 variants from the human T-type calcium channel gene CACNA1G: alternative structures, developmental expression, and biophysical variations. Proteins 64, 320–342.
Fuentealba, P., Timofeev, I., Bazhenov, M., Sejnowski, T.J., Steriade, M., 2005. Membrane bistability in thalamic reticular neurons during spindle oscillations. J. Neurophysiol. 93, 294–304.
Gutierrez, C., Cox, C.L., Rinzel, J., Sherman, S.M., 2001. Dynamics of low-threshold spike activation in relay neurons of the cat lateral geniculate nucleus. J. Neurosci. 21, 1022–1032.
Hernandez-Cruz, A., Pape, H.C., 1989. Identification of two calcium currents in acutely dissociated neurons from the rat lateral geniculate nucleus. J. Neurophysiol. 61, 1270–1283.
Hines, M.L., Carnevale, N.T., 2001. NEURON: a tool for neuroscientists. Neuroscientist 7, 123–135.
Huguenard, J.R., 1996. Low-threshold calcium currents in central nervous system neurons. Annu. Rev. Physiol. 58, 329–348.
Kim, D., Song, I., Keum, S., Lee, T., Jeong, M.J., Kim, S.S., McEnery, M.W., Shin, H.S., 2001. Lack of the burst firing of thalamocortical relay neurons and resistance to absence seizures in mice lacking alpha(1G) T-type Ca(2+) channels. Neuron 31, 35–45.
Kuisle, M., Wanaverbecq, N., Brewster, A.L., Frere, S.G., Pinault, D., Baram, T.Z., Luthi, A., 2006. Functional stabilization of weakened thalamic pacemaker channel regulation in rat absence epilepsy. J. Physiol. 575, 83–100.
Lacey, C.J., Bolam, J.P., Magill, P.J., 2007. Novel and distinct operational principles of intralaminar thalamic neurons and their striatal projections. J. Neurosci. 27, 4374–4384.
Lee, S.H., Govindaiah, G., Cox, C.L., 2007. Heterogeneity of firing properties among rat thalamic reticular nucleus neurons. J. Physiol. 582, 195–208.
Leresche, N., Parri, H.R., Erdemli, G., Guyon, A., Turner, J.P., Williams, S.R., Asprodini, E., Crunelli, V., 1998. On the action of the anti-absence drug ethosuximide in the rat and cat thalamus. J. Neurosci. 18, 4842–4853.
Lo, F.S., Ziburkus, J., Guido, W., 2002. Synaptic mechanisms regulating the activation of a Ca(2+)-mediated plateau potential in developing relay cells of the LGN. J. Neurophysiol. 87, 1175–1185.
Mainen, Z.F., Sejnowski, T.J., 1996. Influence of dendritic structure on firing pattern in model neocortical neurons. Nature 382, 363–366.
Meis, S., Biella, G., Pape, H.C., 1996. Interaction between low voltage-activated currents in reticular thalamic neurons in a rat model of absence epilepsy. Eur. J. Neurosci. 8, 2090–2097.
Meuth, S.G., Kanyshkova, T., Meuth, P., Landgraf, P., Munsch, T., Ludwig, A., Hofmann, F., Pape, H.C., Budde, T., 2006. Membrane resting potential of thalamocortical relay neurons is shaped by the interaction among TASK3 and HCN2 channels. J. Neurophysiol. 96, 1517–1529.
Pape, H.C., 1996. Queer current and pacemaker: the hyperpolarization-activated cation current in neurons. Annu. Rev. Physiol. 58, 299–327.
Pape, H.C., Budde, T., Mager, R., Kisvarday, Z.F., 1994. Prevention of Ca(2+)-mediated action potentials in GABAergic local circuit neurones of rat thalamus by a transient K+ current. J. Physiol. 478 (Pt 3), 403–422.
Paz, J.T., Chavez, M., Saillet, S., Deniau, J.M., Charpier, S., 2007. Activity of ventral medial thalamic neurons during absence seizures and modulation of cortical paroxysms by the nigrothalamic pathway. J. Neurosci. 27, 929–941.
Perez-Reyes, E., 2003. Molecular physiology of low-voltage-activated t-type calcium channels. Physiol. Rev. 83, 117–161.
Perez-Reyes, E., 2006. Molecular characterization of T-type calcium channels. Cell Calcium 40, 89–96.
Pinault, D., O'Brien, T.J., 2007. Cellular and network mechanisms of genetically-determined absence seizures. Thalamus & Related Systems, doi:10.1017/S1472928807000209, 1–23.
Pinault, D., Leresche, N., Charpier, S., Deniau, J.M., Marescaux, C., Vergnes, M., Crunelli, V., 1998. Intracellular recordings in thalamic neurones during spontaneous spike and wave discharges in rats with absence epilepsy. J. Physiol. 509 (Pt 2), 449–456.
Seidenbecher, T., Pape, H.C., 2001. Contribution of intralaminar thalamic nuclei to spike-and-wave-discharges during spontaneous seizures in a genetic rat model of absence epilepsy. Eur. J. Neurosci. 13, 1537–1546.
Seidenbecher, T., Staak, R., Pape, H.C., 1998. Relations between cortical and thalamic cellular activities during absence seizures in rats. Eur. J. Neurosci. 10, 1103–1112.
Sherman, S.M., Guillery, R.W., 2006. Exploring the Thalamus and its Role in Cortical Function. MIT Press, Cambridge, Massachusetts.
Slaght, S.J., Leresche, N., Deniau, J.M., Crunelli, V., Charpier, S., 2002. Activity of thalamic reticular neurons during spontaneous genetically determined spike and wave discharges. J. Neurosci. 22, 2323–2334.
Song, I., Kim, D., Choi, S., Sun, M., Kim, Y., Shin, H.S., 2004. Role of the alpha1G T-type calcium channel in spontaneous absence seizures in mutant mice. J. Neurosci. 24, 5249–5257.
Steriade, M., 1997. Synchronized activities of coupled oscillators in the cerebral cortex and thalamus at different levels of vigilance. Cereb. Cortex 7, 583–604.
Talley, E.M., Cribbs, L.L., Lee, J.H., Daud, A., Perez-Reyes, E., Bayliss, D.A., 1999. Differential distribution of three members of a gene family encoding low voltage-activated (T-type) calcium channels. J. Neurosci. 19, 1895–1911.
Talley, E.M., Solorzano, G., Depaulis, A., Perez-Reyes, E., Bayliss, D.A., 2000. Low-voltage-activated calcium channel subunit expression in a genetic model of absence epilepsy in the rat. Brain Res. Mol. Brain Res. 75, 159–165.
Tennigkeit, F., Schwarz, D.W., Puil, E., 1998. Modulation of bursts and high-threshold calcium spikes in neurons of rat auditory thalamus. Neuroscience 83, 1063–1073.
Tsakiridou, E., Bertollini, L., de Curtis, M., Avanzini, G., Pape, H.C., 1995. Selective increase in T-type calcium conductance of reticular thalamic neurons in a rat model of absence epilepsy. J. Neurosci. 15, 3110–3117.
Van der Werf, Y.D., Witter, M.P., Groenewegen, H.J., 2002. The intralaminar and midline nuclei of the thalamus. Anatomical and functional evidence for participation in processes of arousal and awareness. Brain Res. Brain Res. Rev. 39, 107–140.
van Ooyen, A., Duijnhouwer, J., Remme, M.W., van Pelt, J., 2002. The effect of dendritic topology on firing patterns in model neurons. Network 13, 311–325.
Williams, D., 1953. A study of thalamic and cortical rhythms in petit mal. Brain 76, 50–69.
Williams, S.R., Stuart, G.J., 2000. Action potential backpropagation and somato-dendritic distribution of ion channels in thalamocortical neurons. J. Neurosci. 20, 1307–1317.
Yasukawa, T., Kita, T., Xue, Y., Kita, H., 2004. Rat intralaminar thalamic nuclei projections to the globus pallidus: a biotinylated dextran amine anterograde tracing study. J. Comp. Neurol. 471, 153–167.
Ying, S.W., Abbas, S.Y., Harrison, N.L., Goldstein, P.A., 2006. Propofol block of I(h) contributes to the suppression of neuronal excitability and rhythmic burst firing in thalamocortical neurons. Eur. J. Neurosci. 23, 465–480.
Zhan, X.J., Cox, C.L., Rinzel, J., Sherman, S.M., 1999. Current clamp and modeling studies of low-threshold calcium spikes in cells of the cat's lateral geniculate nucleus. J. Neurophysiol. 81, 2360–2373.
Zhang, Y., Mori, M., Burgess, D.L., Noebels, J.L., 2002. Mutations in high-voltage-activated calcium channel genes stimulate low-voltage-activated currents in mouse thalamic relay neurons. J. Neurosci. 22, 6362–6371.
Zhang, Y., Vilaythong, A.P., Yoshor, D., Noebels, J.L., 2004. Elevated thalamic low-voltage-activated currents precede the onset of absence epilepsy in the SNAP25-deficient mouse mutant coloboma. J. Neurosci. 24, 5239–5248.